JOURNAL OF GEOPHYSICAL RESEARCH, VOL. 94, NO. B7, PAGES 9215–9236, JULY 10, 1989

Dynamic Mixing in Magma Bodies: Theory, Simulations, and Implications

CURTIS M. OLDENBURG AND FRANK J. SPERA

Department of Geological Sciences, University of California, Santa Barbara

DAVID A. YUEN

Minnesota Supercomputer Institute and Department of Geology and Geophysics University of Minnesota, Minneapolis

GRANVILLE SEWELL

Department of Mathematical Sciences, University of Texas, El Paso

Considerable geochemical and petrographic evidence suggests that magma mixing phenomena are important in producing the chemical heterogeneity commonly observed in plutonic and volcanic rocks on a variety of scales in both space and time. Simulations of time-dependent, variable viscosity, double-diffusive convection have been carried out to quantitatively investigate the mixing dynamics of magma in melt-dominated magma bodies. Two distinct measures of the "goodness of mixing" are used to quantify magma mixing: (1) the linear scale of segregation (L) which corresponds to the length scale of a typical compositional anomaly; and, (2) the intensity of segregation (I) which is a measure of the deviation of compositional anomalies from the mean. Nondimensionalization of the governing conservation equations shows that the style and time scale of mixing depend on the flux Rayleigh number ($Rq = \alpha g q d^4/k\kappa\nu_m$), the buoyancy ratio ($Rr = \beta\Delta C k/\alpha q d$), the Lewis number ($Le = \kappa/D$), the silicic to mafic melt viscosity ratio ($\nu_r = \nu_s/\nu_m$), and the aspect ratio ($A = w/d$) of the chamber. Simulations of magma mixing were carried out by solving the conservation equations for parameter ranges $10^5 < Rq < 3 \times 10^5$, $0 < Rr < 1.1$, $100 < Le < 600$, $1 < \nu_r < 20$, $0.3 < A < 3$ by a Galerkin finite element method over a two-dimensional domain with various geologically relevant boundary conditions. The mixing time (t_{mix}) is defined as the time required for the intensity of segregation to decay to a certain value. Magma mixing occurs by complex time-dependent flows with numerous flow reversals associated with local unmixing events superimposed on a larger time scale process in which the intensity of segregation decays to zero. For parameters within the ranges investigated, t_{mix} is roughly proportional to $\nu_r^{1/2} Le^{1/2} Rr^{2} Rq^{-1}$ for the heating from below scenario. For values of ν_r, Le, Rr, and Rq appropriate to natural systems, this relationship gives a range of mixing times from about one tenth to 10 times d^2/κ, implying that both well-mixed and heterogeneous magmas will be commonly observed in nature. Mixing times are at a minimum for equant bodies, while for sill-like bodies, mixing is inhibited by the formation of multiple cells of different composition in the horizontal. Assimilation and fractional crystallization geochemical models that assume "well-mixed" magma bodies may be grossly misleading. A viscous (i.e., crystal laden), large ($d \sim 5$ km) magma body heated weakly from below and initially strongly chemically stratified will remain unmixed for several Ma. A large-volume, thermally well-connected basaltic body will mix rapidly ($10^3 - 10^4$ years). Because flow reversals may occur in dynamic mixing ($Rr > 0$), crystal distributions within convecting magma bodies will be different from those predicted assuming steady state velocity fields. Flow reversals cause significant temporal variation in the heat supplied to the roof of the chamber; these may be important in explaining episodic phases of hydrothermal alteration. In sill-like magma bodies ($A > 2$), multiple cells of distinct composition may persist for geologically significant time periods. Finally, our simulations show that the dynamics of double-diffusive convection can impart complex patterns of composition through time and space in magma bodies.

INTRODUCTION

A large amount of volcanological, geochemical, and petrological evidence points toward the importance of magma mixing in explaining the chemical heterogeneity found in many igneous rocks. Documentation of specific cases and general reviews of magma mixing have been discussed extensively through the years [e.g., *Wilcox*, 1954; *Walker and Skelhorn*, 1966; *Eichelberger*, 1975; *Vernon*, 1983; *Furman and Spera*, 1985; *Bacon*, 1986; *Sparks and Marshall*, 1986; *Grove et al.*, 1989]. Evidence of magma mixing is observed in both plutonic and volcanic rocks across the entire compositional range relevant to petrogenesis, although composite lava or mixed pumice provides the only unequivocal evidence of the process [*Green*, 1988]. Presented in Table 1 is a summary of the many different kinds of heterogeneities which can be caused by magma mixing. Of particular note in Table 1 is the wide range of characteristic length scales of the heterogeneities.

Paper number 89JB00327.
0148-0227/89/89JB-00327$05.00

Table 1.

Heterogeneity		Scale, m	Selected References
Plutonic	Volcanic		
Zoning, cryotic zoning	Zoning, cryptic, zoning, melt inclusions	$<10^{-3}$	7, 14, 10, 1
Xenocrysts, mafic clots	Xenocrysts	$10^{-3} - 10^{-2}$	5, 6, 2
Mafic enclaves, schlieren	Mixed pumice, inclusions	$10^{-2} - 1$	3, 4, 13, 9, 6
Dike swarms, enclave swarms	Zonation in lava flows and ash flow tuffs	1 – 10	4, 15, 11, 18
Plutonic complexes	Zonation in large volume ash flow tuffs	$10 - 10^4$	16, 17, 12, 8

1, *Dungan* [1987]; 2, *Eichelberger* [1975]; 3, *Frost and Mahood* [1987]; 4, *Furman and Spera* [1985]; 5, *Gibson and Walker* [1963]; 6, *Grove et al.* [1989]; 7, *Hibbard* [1981]; 8, *Hildreth* [1979]; 9, *Hildreth* [1983]; 10, *Pallister and Hopson* [1981]; 11, *Reagan et al.* [1987]; 12, *Smith* [1979]; 13, *Vernon* [1983]; 14, *Wiebe* [1968]; 15, *Wiebe* [1973]; 16, *Wiebe* [1974]; 17, *Wiebe* [1980]; 18, *Wright* [1973] .

The concept of the length scale of the heterogeneity is an important part of this paper which we will return to when convective magma mixing is discussed in quantitative terms.

The quantitative study of convective magma mixing is complicated by uncertainty about most of the potentially critical factors. These include, for instance, the transport properties of the mixing magmas (e.g., viscosity, chemical diffusivities), the relative importance of chemical diffusion versus shear and normal strain during mixing, the role of chemical and thermal buoyancy, the configuration of the magma interaction, and very important, the boundary and initial conditions of the system. Consequently, the goal of this work is to investigate a few specific and plausible scenarios for convective magma mixing within a chamber and to develop a quantitative relationship between the "goodness of mixing" (discussed below) and the parameters of the problem.

The goodness of mixing refers to two conceptually distinct measures of the composition field: (1) the scale of segregation and (2) the intensity of segregation [*Danckwerts*, 1952]. The linear (or volumetric) scale of segregation refers to the size spectrum of the compositional heterogeneities. In Table 1, for example, the length scale given corresponds in a general way to the linear scale of segregation, which is rigorously defined in a later section. For the moment, one may ignore the effects of chemical diffusion and consider the evolution of the size spectrum of the compositional anomalies (i.e., the clumps of melt of different composition) through time. At the outset, the two components occupy distinct regions of space; the action of convective mixing is to reduce the size of the compositional anomalies through time. A crude analogy is the behavior of caramel swirls in an otherwise homogeneous batch of vanilla ice cream. If the swirls break up, the average size (say, volume to the 1/3 power) of the caramel swirls is reduced during stirring. The second aspect of the goodness of mixing refers to the intensity of segregation. Without diffusion, the vanilla ice cream and caramel swirls will always remain distinct; at any location in space and time, either pure vanilla ice cream or pure caramel is found. In this case the intensity of segregation is constant and remains at its maximum value throughout the mixing event. In reality, however, diffusion plays a role once the sizes of the caramel swirls have been reduced to diffusive length scales. In this case, the composition of fluid at some position and time will be intermediate between the two pure mixing components, and therefore the intensity of segregation is reduced.

The above formalism facilitates the quantification of convective mixing. In the two-dimensional simulations presented here, mixing occurs by both diffusion and shear and normal strains induced by convection in a magma body which initially consists of a layer of silica-rich magma above a more mafic magma. We shall refer hereafter to the two magmas as being silicic and mafic, although nothing specific is implied about their silica contents; all that is implied by these terms is that at the same temperature, the silicic magma has lower density than the mafic magma. Because of the action of normal and shear strains, the average size of entrained clumps decreases through time although not uniformly. The silicic melt in the upper layer has higher viscosity and lower density relative to mafic melt at the same temperature. Hence a tendency to resist deformation and entrainment also exists. The mixing history is consequently directly related to the competition between thermally driven convective motions which tend to homogenize melt and gravitational forces associated with compositional buoyancy which tend to maintain a segregated compositional field. Chemical diffusion plays a role in the mixing process once the effects of shear and normal strain have reduced the size of a compositional anomaly sufficiently. For a typical species in a melt at low to moderate pressure, the diffusive length scale is approximately 1 m for a characteristic time of 10^5 years. Mixing by normal and shear strains (Olson et al., 1984*a*) will usually greatly dominate over diffusion; this is a well-known result, illustrated in previous studies concerned with the mixing of passive heterogeneities in the mantle of the

Earth [e.g., *McKenzie*, 1979; *Richter et al.*, 1982; *Olson et al.*, 1984*a*, *b*; *Hoffman and McKenzie*, 1985; *Gurnis and Davies*, 1986].

The magma mixing problem is somewhat different from mantle mixing problems. In magma mixing, the mixing components (e.g., silicic and mafic melt) are dynamically active in the sense that the melt density depends strongly on composition. In addition, the mixing components affect magma viscosity. This is not the case in a passive tracer dispersion problem as appropriate in mantle mixing. The magma mixing problem is essentially a problem in multicomponent convection but will be treated in this study as double-diffusive convection. Aside from experimental work with aqueous solutions [e.g., *Huppert and Sparks*, 1980; *Olson*, 1984; *Turner and Cambell*, 1986; *Martin and Campbell*, 1988] and a high-temperature experiment on magma mixing by forced convective stirring [*Kouchi and Sunagawa*, 1983], the dynamics of magma mixing at convective time scales (10^2–10^6 years) have not received much quantitative attention despite abundant geochemical data supporting the general concept of magma mixing.

Although one may incorporate many of the important complexities of magma body evolution such as crystallization, conjugate hydrothermal convection, and time dependent boundary conditions into the current generation of simulation studies (and some of these complexities will be introduced below) the immediate goals of this paper are to (1) discuss the geological motivation for the magma mixing scenario investigated, (2) establish quantitative criteria of practical use to the petrologist for describing the goodness of mixing of any magma, (3) show how the rate of mixing of an initially completely segregated, melt-dominated, compositionally zoned magma body depends on the transport and thermodynamic properties of magma, the shape of the magma body, and the choice of boundary and initial conditions, and (4) discuss some of the important petrologic implications of this work.

Finally, it should be noted that there is little hope of understanding the dynamics of mixing of a rheologically complex fluid (i.e., magma) in an irregular container of constantly changing shape and size (i.e., a magma chamber) in which simultaneous assimilation, crystal fractionation, and magma replenishment may be occurring without first understanding a few simple cases. For even if one knew the exact physical properties and boundary and initial conditions appropriate for natural magmatic systems, present limitations in computing power would prevent the exact numerical simulation of the system. Starting with a simplified mixing scenario, we will study the effects of various physical properties and boundary conditions on the convective mixing process. Our results will be useful as a guide to future simulation work on systems more closely resembling natural magma bodies.

GEOLOGIC SETTING

The model magma body investigated in this study is based on inferences drawn from many detailed volcanological, petrological, and geochemical studies of ash flow magmatism [e.g., *Smith*, 1979; *Hildreth*, 1981; *Bacon*, 1983; *Crisp* and *Spera*, 1987], and is shown schematically in Figure 1. Large-volume, phenocryst-poor magma

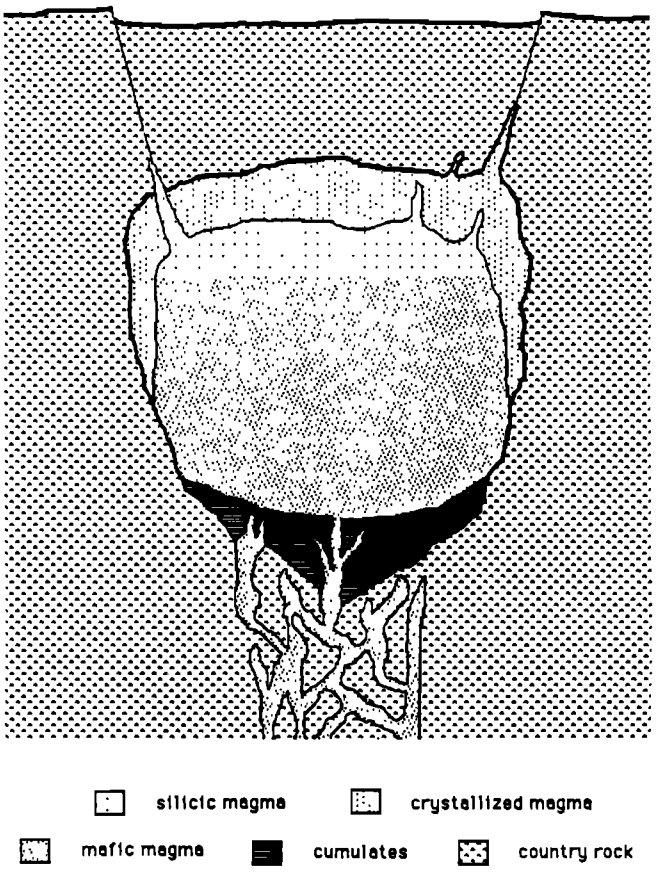

Fig. 1. Generalized cross section of stratified crustal magma body showing basal feeder zone, zone of cumulates, main body of mafic magma, cap of silicic magma, and crystallized roof zone. No specific scale is intended.

reservoirs are widely believed to have been the source of the voluminous pyroclastic flow sheets so common throughout the geological record. The problem of the origin of compositional zonation in crustal magma bodies has received a great deal of attention [e.g., *Shaw*, 1974; *Turner*, 1980; *McBirney*, 1980; *Hildreth*, 1981; *Spera et al.*, 1984; *Lowell*, 1985; *Nilson et al.*, 1985; *McBirney et al.*, 1985; *Trial and Spera*, 1988], although a rigorous, correctly scaled quantitative theory remains lacking. In general, there are two ways by which the "light above heavy" arrangement may come into being: (1) partial fusion induces density stratification ab initio or (2) stratification develops in situ from an originally homogeneous magma. In the first process, a progressive increase in the density of partial melt is the result of rapid relative depletions of large partial molar volume components (e.g., H_2O, K_2O, Na_2O, CO_2) from the source during progressive partial fusion. Some experimental support for this process was noted by *Dowty and Berkebile* [1982]. A popular form of the second process is the boundary layer crystallization or assimilation hypothesis whereby buoyant melt generated along vertical or sloping sidewalls migrates upward and accumulates in the upper parts of a magma body.

Although a consensus as to what produces compositional structure has yet to be reached, it is an inescapable conclusion that the source bodies of many large-volume pyroclastic flow eruptions are heterogeneous. Similarly, the

relative volumes of silicic to mafic magma contained within magma bodies are not known precisely, although a conventional view is that the silicic to mafic ratio is rather small [*Smith*, 1979; *Hildreth*, 1981].

The thermal conditions of large magma bodies are currently the subject of much interest. Clearly, magma bodies cool while in the upper crust. And they do so through their lateral and upper margins with varying degrees of efficiency, depending on the ability of the wall rock to transfer heat away from the body by either hydrothermal convection [*Norton and Knight*, 1977; *Bejan and Anderson*, 1983] or heat conduction [*Carrigan*, 1987]. The lower margins are more complex. Some magma bodies are undoubtedly thermally well connected to hotter inputs of magma. Many examples of thermally well connected systems have been documented in the literature; two recent examples include the studies of *Nixon* [1988*a*, *b*] and *Wiebe* [1988]. If there are episodic heat inputs to the floor of the body, the basal heat flux due to magma replenishment at volumetric rate $\dot{V}$ is $q = \rho \dot{V} C_p \Delta T / A_c$. If magma is supplied to the chamber at a time-averaged rate ($\dot{V}$) of 5 x 10^{-3} km^3 yr^{-1}, a value consistent with observations [*Shaw*, 1973; *Hardee*, 1982; *Crisp*, 1984], then a flux of about 200 mW m^{-2} (~5 HFU where 1 HFU = 10^{-6} cal cm^{-2} s^{-1}) is delivered to the body, assuming ρ = 2800 kg m^{-3}, C_p = 1200 J kg^{-1} K^{-1}, ΔT = 10 K, and the basal surface area (A_c) is 25 km^2. This neglects the contribution due to latent heat which would increase the available enthalpy. Perhaps other magma bodies are thermally disconnected, in which case they cool out the floor in addition to cooling out the sides and roof. We have investigated both types of boundary conditions in this paper, although most of our results are for the heating from below case. In either case, convection and subsequent convective mixing are inevitable results of the emplacement of magma into cooler surroundings.

The model magma body considered in this study is melt dominated, of fixed aspect ratio ($A = w/d$, where w is width and d is depth of the chamber) with rigid walls, and initially has a horizontal, compositionally buoyant cap. Initially, the upper one-fifth of the body consists of viscous silicic melt; the remaining portion consists of less viscous mafic component. The 1:4 ratio of silicic to mafic magma was chosen arbitrarily to provide more mafic than silicic magma. The initial temperature profile in the body is either linear or steplike. With the objective of investigating how long it takes for the body to mix by convection, the system is "turned on" at t = 0 and the temporal development of the velocity, temperature, and composition fields is followed for various imposed fluid, boundary, and geometric conditions.

The volume and bulk composition of magma within the body do not change during the mixing process. Assimilation and fractional crystallization are not taken into account, although as indicated above, it is possible that these processes may give rise to the composition field taken here as the initial condition. The impermeability of the chamber margins was chosen to isolate the effects of internal convective dynamics from the additional complexities of mass transfer across the boundaries of the system.

Several of the many possible thermal boundary conditions have been investigated. In all cases, we consider cooling out of the roof of the body. In most cases, the roof of the chamber defines an isotherm, taken to be the solidus temperature of melt of granitic bulk composition. This ignores latent heat effects and solidification and melting at the chamber roof. In other cases, a constant heat flux out through the roof consistent with the notion of conduction-limited cooling is imposed. Cooling through the roof, independent of any other thermal condition on any other boundary, will result in natural convection if the cooling is of sufficient magnitude. The style and vigor of convection will depend, however, on the thermal conditions imposed on the lateral and bottom margins. We have investigated the convective mixing resulting from cooling through the roof with heating from below, and cooling through the roof and sides with heating from below, and cooling through all four boundaries (roof, sides, and floor).

To simulate thermally well-connected magmatic systems, we impose a heat flux along the floor of the body. If a time-dependent heat flux is used, as may be appropriate for episodic influxes of hot magma, an arbitrary periodicity, difficult to justify a priori, is introduced by the form and magnitude of the heat flux function. In the mixing of a dynamically active component by convection, periodicity associated with reversals of flow occurs naturally. In order to learn about these natural periodicities, it is advantageous to impose a constant heat flux in the bottom. We experimented with a basal heat flux which was dependent on the square root of time and found, as expected, the mixing time was a bit longer than for the constant heat flux case. For most of our work, a constant heat flux into the chamber is imposed through the floor of the body. In this way, the flow reversals and other time-dependent dynamic features observed are intrinsic to double-diffusive convection and not artifacts of arbitrarily chosen time-dependent boundary conditions. Also, it should be noted that the initial temperature profiles in the body cause the convective mixing in the heating from below scenario to be a net cooling problem; the total heat content at steady state in the body is about one-third the initial heat content.

To simulate thermally disconnected magmatic systems, several calculations were made with cooling out all surfaces of the body. Again, mixing is slower in this scenario. However, it will be shown in a later section that the difference between mixing times for the case where there is cooling out all margins and for the case where there is cooling only out the top is small. Similarly, the dependence of mixing time on fluid properties (e.g., viscosity ratio, thermal to chemical diffusivity ratio) does not seem to be greatly affected by boundary conditions, although more simulations are needed to understand this matter more completely. Because the Rayleigh number and chemical to thermal buoyancy ratio contain quantities specified at the boundaries, their effects on the mixing time will change with boundary conditions.

CONVECTIVE MIXING

Introduction

It is important to note that two different concepts contribute to what is normally meant by the goodness of mixing. One is the length scale or size of compositional anomalies; this defines the scale of segregation defined in terms of the size spectrum of the ensemble of compositional anomalies. The other is the contrast, or deviation in

composition at some arbitrary location, relative to the mean composition of the magma body; this is the intensity of segregation defined in terms of the variance (in the statistical sense) of the composition field. At length and time scales where interspecies diffusion is unimportant, the linear scale of segregation (L) will decrease with time, although not necessarily monotonically. If diffusion plays no role in the mixing, the mixture remains compositionally "grainy" throughout the mixing event. The intensity of segregation is at a maximum (unity) and remains constant when diffusion is not important.

A rigorous method for describing magma mixing is necessarily based on statistical methods. The procedure adopted here follows from the work of *Taylor* [1935] and *Danckwerts* [1952] and is formally related to the statistical theory of turbulence as summarized, for example, by *Batchelor* [1953]. A good review of the laminar mixing process is given by *Ottino and Chella* [1983]. The two distinct measures of the goodness of mixing, the scale and intensity of segregation, are discussed in turn below.

First, we define the nondimensional compositional variable, $\hat{C}$:

$$\hat{C} = \frac{C - C_m}{C_s - C_m} \tag{1}$$

where C_m and C_s represent the mass fraction of some component, say, SiO_2, in mafic and silicic melts, respectively, and $C(x, y, t)$ is the concentration (mass fraction) of silica at some location (x, y) and time (t) after juxtaposition of the two compositionally distinct melts. Note that $\hat{C}$ varies between unity (pure "rhyolite") and zero (pure "basalt") and depends on location within the chamber and the duration of the mixing event. For the 4:1 mafic to silicic ratio assumed throughout this study, the spatially averaged magma composition, denoted by $\hat{C}_{av}$, is constant and equal to 0.2 at all times.

Scale of Segregation

Consider a mixture of two components, S and M, in which S is identified as the buoyant component. Without loss of generality, the dimensionless concentration of component S as defined in (1) may be used to describe the melt composition at any point. Now, suppose the concentration of component S is measured at two locations in the fluid a distance r apart at some time t. If $\hat{C}_1$ and $\hat{C}_2$ represent the concentrations at the two points, the deviations from the mean form the product

$$(\hat{C}_1 - \hat{C}_m)(\hat{C}_2 - \hat{C}_m) \tag{2}$$

If a large number of such pairs are taken, with the points in each pair being a distance r apart, one may calculate the mean value of the products of the deviations. This quantity is known as the space correlation and is written

$$R^*(r) = \overline{(\hat{C}_1 - \hat{C}_m)(\hat{C}_2 - \hat{C}_m)} \tag{3}$$

The overbar implies a spatial average has been taken. One may also calculate the variance (second moment) of the composition field (measured about the mean) according to

$$\sigma^2 = \frac{1}{N-1}\sum_{i=1}^{N}(\hat{C}_i - \hat{C}_m)^2 \tag{4}$$

where $\hat{C}$ is known at N discrete locations within the mixing region. It is useful to define several higher moments of the compositional field in addition to the variance. The skewness or third moment of the composition ($\hat{C}$) field is defined according to

$$m_3 = \frac{1}{N}\sum_{i=1}^{N}\left(\frac{\hat{C}_i - \hat{C}_m}{\sigma}\right)^3 \tag{5}$$

where σ is the standard deviation of the $\hat{C}$ field. A positive value of the skewness implies a frequency distribution of composition with an asymmetric tail extending out toward more silicic compositions; a negative value signifies a distribution with a long tail toward more mafic ones. The fourth moment, or kurtosis (m_4), measures the peakedness ($m_4 > 0$) or flatness ($m_4 < 0$) of a distribution relative to a normal distribution. The kurtosis (m_4) is defined

$$m_4 = \frac{1}{N}\sum_{i=1}^{N}\left(\frac{\hat{C}_i - \hat{C}_m}{\sigma}\right)^4 - 3 \tag{6}$$

Note that $m_4 = 0$ for normal (Gaussian) distribution.

Based on (2)–(4), the composition correlation function for all values of $\hat{C}$ a distance r apart is

$$R(r) = \frac{R^*(r)}{\sigma^2} \tag{7}$$

The correlation function $R(r)$ reflects the effects of both chemical diffusion (through the variance) and mixing by convectively driven shear and normal strain rate fields. $R(r)$ is interpreted in a manner analogous to the velocity correlation function in statistical theories of turbulence [*Taylor*, 1935]. In the application to two-component mixing $R(r)$ may take on any value between 1 and -1. A value close to 1 means that a concentration greater or less than the mean at some point in the fluid is likely to be correlated with a similar positive or negative compositional anomaly a distance r away. A value near zero means that there is a random relationship between the concentrations at the two locations a distance r apart. A value near -1 means that there is a perfect anticorrelation between the fluid compositions at the two locations; for instance, if pure "rhyolite" is at one location, then pure "basalt" is at the other. In Figure 2, the composition correlation function is shown for the initial configuration of the model system shown in Figure 3 (cf. Figure 1). There is a nearly linear relationship between $R(r)$ and the separation distance (r) in the interval $r = 0$ to $r \approx 0.8$ which reflects the initial large-scale segregation. Note also the rapid changes in dR/dr near $r = 0.2$ and $r = 0.8$. For pairs with $r > 0.8$, a nearly perfect anticorrelation exists. The structure of the initial composition field is clearly reflected in the shape of the compositional correlation function $R(r)$.

The correlation function indicates the distance over which the composition at one point affects that at another. It may

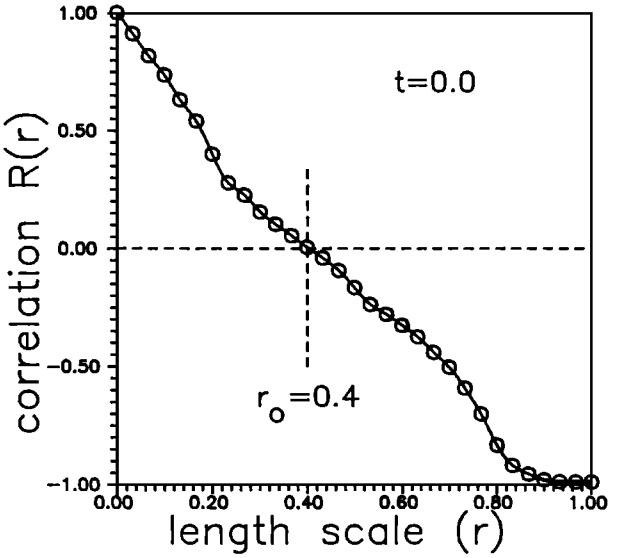

Fig. 2. Correlogram of composition $\hat{C}$ for the mixing system at $\hat{t}$ = 0.0. Changes in slope of the correlogram at r = 0.20 and r = 0.80 reflect the step in composition at $\hat{y}$ = 0.80 of the initial configuration. For $R(r) > 0$, positive correlation of compositions exists; for $R(r) < 0$, negative correlations exist. When $r > 0.80$, perfect anticorrelation exists, reflecting the initial step in composition. The value of r at which the correlation is random (R = 0) is denoted by r_o and is equal to 0.4 at $\hat{t}$ = 0.0.

be used to assign a length scale for the compositional anomaly. One scale, the linear scale of segregation (L), is defined

$$L = \int_0^{r=r_o} R(r)\, dr \qquad (8a)$$

where r_o is the minimum value of r at which the correlation function equals zero (Figure 2). A related scale is the volume scale of segregation (V) defined

$$V = 2\pi \int_0^{r=r_o} r^2 R(r)\, dr \qquad (8b)$$

Because the ratio L/V is independent of the variance, it provides information about the deformation of compositional anomalies. In our simulations, L/V increases when the upper layer becomes entrained into the main flow. An additional useful scale, based on the space correlation alone, is defined

$$L^* = \int_0^{r=r_o} R^*(r)\, dr = \sigma^2 L \qquad (9)$$

Intensity of Segregation

The intensity of segregation is convienently measured by the globally averaged variance of the composition. If the variance at any t is divided by its initial value, the resulting ratio is the intensity of segregation (I)

$$I = \frac{\sigma^2}{\hat{C}_{av}(1-\hat{C}_{av})} \qquad (10)$$

where $\hat{C}_{av}$ is the average concentration of the buoyant component. For the initial and boundary conditions of Figure 1, $\hat{C}_{av}$ = 0.2. Note that in the absence of diffusion, I = 1 throughout the mixing event.

In summary, once the composition field has been calculated, it is possible to define the goodness of mixing in terms of a scale (L or L^*) and an intensity (I) of segregation. The goodness of mixing is therefore seen to depend on both the space correlation and the second moment of the composition field. The space correlation gives information on the probability that a positive (negative) composition fluctuation at one point is correlated with a positive (negative) anomaly a distance r away. In any flow with nonzero diffusion effects, $I \to 0$ as $t \to \infty$. This is because once normal and shear strains have reduced an intense compositional anomaly to a diffusive length, it will be erased. As $t \to \infty$, $L^* \to 0$ and $L(=L^*/\sigma^2)$ tends toward a small constant which is related to the minimum resolvable length scale implied by the spatial resolution of the model (i.e., the number of nodes employed in the simulation). For the simulations reported here the minimum resolvable scale lies between 1/30 and 1/60 of the characteristic chamber dimension.

The evolution of $R(r)$, $L(t)$, $L^*(t)$, $\sigma^2(t)$ and the other statistics during a mixing process provides quantitative information on the size spectrum and intensity of the compositional anomalies. Note that these statistical measures may be calculated or measured for any exposed pluton, ignimbrite, or lava flow provided sufficient geochemical data are available. Note also that the length scales given in Table 1 correspond approximately to L. A statistical treatment of the moments and space correlation of the compositional field of an igneous body enables one to quantitatively define how well mixed the body is at every resolvable length scale.

With the above formalism, several of the terms which have been used to describe the interactions of one or more magmas can be rigorously defined. For example, commingling occurs when two magmas interact in such a way that some of each of the mixing components remains

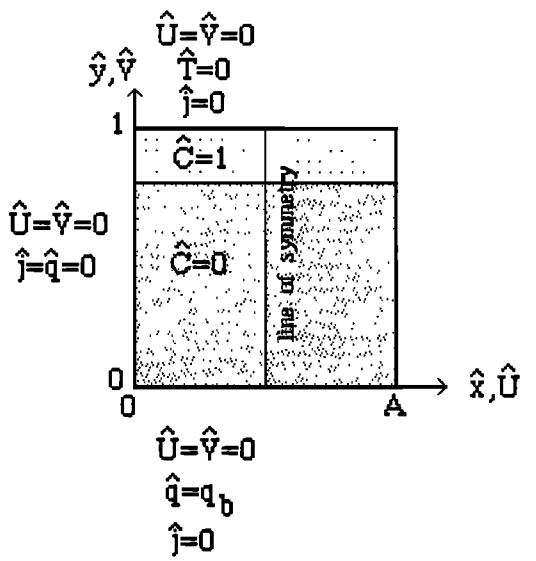

Fig. 3. Approximation to geologic conditions depicted in Figure 1. The computational domain is shown with one set of boundary conditions, coordinate system, and initial condition on composition. Symbols are defined in the notation list.

distinct in the mixture. In such cases the variance remains large ($I \approx 1$) and the mixture is grainy. The scale of heterogeneities is given by the scale of segregation which would be of order 0.1 to 1 m for commingling on the outcrop scale. Hybridization is a process where the intensity or variance goes to zero and the mixture is homogeneous and of composition intermediate between the mixing components. As a working definition, we define the general term magma mixing to be the process of two or more magmas coming together and interacting such that either the intensity or scale of segregation decreases.

NUMERICAL SIMULATIONS

Conservation Equations

The equations governing the evolution of the velocity, temperature, and composition fields in two-component double-diffusive convection include expressions for the conservation of mass, energy, momentum, and species. Convection in this system is double-diffusive because two quantities (heat and SiO_2, or heat and H_2O, etc.) diffuse through the fluid and affect the density of the fluid. The Boussinesq equations governing double-diffusive convection of an infinite Prandtl number fluid with compositionally dependent viscosity in a two-dimensional reservoir are as follows:

Continuity

$$\frac{\partial u}{\partial x} + \frac{\partial v}{\partial y} = 0 \tag{11}$$

x-Momentum

$$0 = \frac{-\partial p}{\partial x} + \frac{\partial \tau_{xx}}{\partial x} + \frac{\partial \tau_{yx}}{\partial y} \tag{12}$$

y-Momentum

$$0 = \frac{-\partial p}{\partial y} + \frac{\partial \tau_{xy}}{\partial x} + \frac{\partial \tau_{yy}}{\partial y} + \rho_o g[\alpha(T - T_o) + \beta(C - C_o)] \tag{13}$$

Energy

$$\frac{\partial T}{\partial t} + u\frac{\partial T}{\partial x} + v\frac{\partial T}{\partial y} = \kappa\left(\frac{\partial^2 T}{\partial x^2} + \frac{\partial^2 T}{\partial y^2}\right) \tag{14}$$

Species conservation

$$\frac{\partial C}{\partial t} + u\frac{\partial C}{\partial x} + v\frac{\partial C}{\partial y} = D\left(\frac{\partial^2 C}{\partial x^2} + \frac{\partial C}{\partial y^2}\right) \tag{15}$$

A linear constitutive relationship (Newtonian viscosity) is employed throughout the numerical experiments with a viscosity that depends upon composition according to a simple exponential law consistent with laboratory studies of melt viscosity [e.g., *Shaw*, 1972; *Urbain et al.*, 1982; *Spera et al.*, 1988]. The elements of the viscous stress tensor become

$$\tau_{xx} = 2\eta_o \frac{\partial u}{\partial x}\exp(B\,(C - C_o)) \tag{16a}$$

$$\tau_{xy} = \tau_{yx} = \left(\frac{\partial u}{\partial y} + \frac{\partial v}{\partial x}\right)\eta_o \exp(B\,(C - C_o)) \tag{16b}$$

$$\tau_{yy} = 2\eta_o \frac{\partial v}{\partial y}\exp(B\,(C - C_o)) \tag{16c}$$

Over a small temperature range (≈200 K) the effects of T on magma viscosity may be accounted for by a simple extension to (16) easily incorporated into the model [e.g., *Spera et al.*, 1982].

In Figure 3 the computational domain is shown along with the common initial and boundary conditions. The velocity field is set to zero everywhere at $t = 0$. The parameters appearing in equations (11)–(16) are defined in the notation list. The equation of state used in all calculations is a modified Boussinesq one in which $\rho = \rho_o[1 - \alpha(T - T_o) - \beta(C - C_o)]$ where α and β represent the coefficients of thermal and compositional expansion and ρ_o is the density of melt of composition C_o and temperature T_o. For the case considered here the reference composition (C_o) and temperature (T_o) are C_m and T_S, respectively. This is the same equation of state used in previous double-diffusion studies [e.g., *Clark et al.*, 1987; *Hansen and Yuen*, 1987]. Values of β for the major oxide components of rhyolitic and basaltic melts at high temperatures may be found in *Clark et al.* [1987].

The dimensional conservation equations are made dimensionless by the following normalizations:

$$\hat{x} = x/d \qquad \hat{u} = du/\kappa$$

$$\hat{t} = \frac{\kappa}{d^2}t \qquad \hat{T} = \frac{(T-T)k}{dq_b}$$

$$\hat{y} = y/d \qquad \hat{v} = dv/\kappa \tag{17}$$

$$\hat{p} = \frac{pd^2}{\eta_o \kappa} \qquad \hat{C} = \frac{C-C_m}{C_i C_m}$$

Substitution of (17) into (11)–(16) results in the nondimensional form of the equations of change applicable to the convective mixing of magmas. These equations are

$$\frac{\partial \hat{u}}{\partial \hat{x}} + \frac{\partial \hat{v}}{\partial \hat{y}} = 0 \tag{18}$$

$$0 = \frac{-\partial \hat{p}}{\partial \hat{x}} + \frac{\partial}{\partial x}\left(2\frac{\partial \hat{u}}{\partial \hat{x}}\exp(b\hat{C})\right) + \frac{\partial}{\partial \hat{y}}\left[\left(\frac{\partial \hat{u}}{\partial \hat{y}} + \frac{\partial \hat{v}}{\partial \hat{x}}\right)\exp(b\hat{C})\right] \tag{19}$$

$$0 = \frac{-\partial \hat{p}}{\partial \hat{y}} + \frac{\partial}{\partial \hat{x}}\left[\left(\frac{\partial \hat{u}}{\partial \hat{y}} + \frac{\partial \hat{v}}{\partial \hat{x}}\right)\exp(b\hat{C})\right] + \frac{\partial}{\partial \hat{y}}\left(2\frac{\partial \hat{v}}{\partial \hat{y}}\exp(b\hat{C})\right) + Rq[\hat{T} + R\hat{r}(\hat{C}-1)] \tag{20}$$

$$\frac{\partial \hat{T}}{\partial \hat{t}} + u\frac{\partial \hat{T}}{\partial \hat{x}} + v\frac{\partial \hat{T}}{\partial \hat{y}} = \frac{\partial^2 \hat{T}}{\partial \hat{x}^2} + \frac{\partial^2 \hat{T}}{\partial \hat{y}^2} \tag{21}$$

$$\frac{\partial \hat{C}}{\partial \hat{t}} + u\frac{\partial \hat{C}}{\partial \hat{x}} + v\frac{\partial \hat{C}}{\partial \hat{y}} = \frac{1}{Le}\left(\frac{\partial^2 \hat{C}}{\partial \hat{x}^2} + \frac{\partial^2 \hat{C}}{\partial \hat{y}^2}\right) \quad (22)$$

The parameters of this problem consist of five nondimensional quantities: a thermal Rayleigh number based on the heat flux imposed along the base or "floor" of the chamber, $Rq = g\alpha q_b d^4/k\kappa\nu$; the ratio of chemically induced stabilizing buoyancy to the destabilizing thermal buoyancy, $Rr = \beta(C_s - C_m)\, k/\alpha q_b d$; the ratio of thermal to chemical diffusivity, the Lewis number ($Le = \kappa/D$), the aspect ratio ($A = w/d$) of the chamber, and the viscosity ratio ($\nu_r = \exp(b)$). It is useful to define the Nusselt number, a measure of the vigor of convection, according to

$$Nu = \overline{(\partial \hat{T}/\partial \hat{y})}_{\hat{y}=1} / \overline{\hat{T}}_{\hat{y}=0} \quad (23)$$

where the overbars denote a spatial average has been taken at the surface. Nu measure the total heat transported by the convecting fluid relative to the heat transported by conduction.

Boundary and Initial Conditions

Several different boundary conditions have been used. Unless stated otherwise, the boundary conditions assumed are

$$\frac{\partial \hat{T}}{\partial \hat{x}} = \frac{\partial \hat{C}}{\partial \hat{x}} = \hat{u} = \hat{v} = 0 \qquad \hat{x} = 0 \quad (24a)$$

$$\frac{\partial \hat{T}}{\partial \hat{x}} = \frac{\partial \hat{C}}{\partial \hat{x}} = \hat{u} = \frac{\partial \hat{v}}{\partial \hat{x}} = 0 \qquad \hat{x} = A/2 \quad (24b)$$

$$\frac{\partial \hat{T}}{\partial \hat{y}} = 1 \qquad \frac{\partial \hat{C}}{\partial \hat{y}} = \hat{u} = \hat{v} = 0 \qquad \hat{y} = 0 \quad (24c)$$

$$\hat{T} = \frac{\partial \hat{C}}{\partial \hat{y}} = \hat{u} = \hat{v} = 0 \qquad \hat{y} = 1 \quad (24d)$$

Results of simulations with other boundary conditions are presented in a later section.

The initial conditions on $\hat{C}$ are

$$\hat{C} = 1 \quad 0 \le \hat{x} \le A \quad 4/5 \le \hat{y} \le 1$$
$$\hat{C} = 0 \text{ for other } (\hat{x}, \hat{y}) \quad (25a)$$

This defines a 1:4 ratio of silicic to mafic melt as indicated in Figures 1 and 3. The initial conditions on $\hat{T}$ are either

$$\hat{T} = 0 \quad 0 \le \hat{x} \le A \quad 4/5 \le \hat{y} \le 1$$
$$\hat{T} = 1 \quad 0 \le \hat{x} \le A \quad 0 \le \hat{y} \le 4/5 \quad (25b)$$

or

$$\hat{T} = 1 - \hat{y} \quad 0 \le \hat{x} \le A \quad 0 \le \hat{y} \le 1 \quad (25c)$$

The initial condition (25b) corresponds to a step change in $\hat{T}$ across the chemical interface; in (25c), $\hat{T}$ is assumed linear. Mixing is found to proceed more rapidly (by about a factor of 2) in the step $\hat{T}$ case. We have adopted the conservative approach and assume condition (25c), although a number of cases with the step $\hat{T}$ profile have also been studied.

Simulation Algorithm

Equations (18)–(22) subject to the appropriate boundary and initial conditions were solved as a function of time for a range Rq, Le, Rr, A (aspect ratio), and viscosity ratio (ν_r). Because of the symmetry about the line $\hat{x} = A/2$, the computational domain (Figure 3) is one half the size of the magma body (cf. Figures 1 and 3). We have verified that symmetry is preserved by running some cases with the full domain. Solution of the discretized versions of (18)–(22) was accomplished by a Galerkin finite element method. The algorithm employs triangular finite elements with quadratic basis functions. The resulting set of algebraic equations is solved by Newton's method. An implicit scheme for advancing in time is used in the time-dependent equations. Details of the algorithm are given in the monograph by *Sewell* [1985].

The solution of differential equations by numerical methods involves discretizing the domain and solving the equations at a finite number of points or nodes. The coarsest discretization used here has 400 elements (841 nodes), and the finest used has 1600 elements (3281 nodes). As a consequence, the model resolves lengths from 1/30 in the coarse discretization to about 1/60 in the fine discretization of the characteristic chamber dimension (d). Practical limitations on CPU time generally restrict solutions to this order of spatial resolution.

To verify the accuracy and resolution of a solution, simulations were run with various discretizations (e.g., about 400, 800, 1600 finite elements). Solutions were deemed accurate provided the field variables differed by less than a few percent upon doubling the number of elements. Additional tests were run using different time increments to insure the veracity of the temporal development of the $\hat{C}$, $\hat{T}$ and velocity fields.

The criterion used for terminating a simulation was that the variance (σ^2) of the composition field be less than or equal to 0.0025, which is equivalent to an intensity (I) of 0.016. The mixing time ($\hat{t}_{mix}$ is defined as the time at which σ^2 equals 0.0025 (i.e., standard deviation (σ) = 0.05). For the 4:1 mafic/silicic bulk composition, this criterion means that for "andesite-basalt," "dacite-basalt," and "dacite-andesite" mixing couples, the system is mixed when the standard deviations of the SiO_2 content are 0.5, 0.75, and 0.2 wt %, respectively. These limits are close to analytical uncertainties. Note that the criterion used to establish the mixing time is based solely on the intensity of segregation.

RESULTS

Mixing Evolution

In Figures 4, 5, and 6 the temporal evolution of a typical convective mixing episode is graphically portrayed. The boundary conditions are identical with those in Figure 3; the initial temperature profile is linear ($\hat{T} = 1 - \hat{y}$). The simulation parameters are $Rq = 2 \times 10^5$, $Rr = 0.25$, $Le = 200$, $A = 1$, and the viscosity ratio (ν_r) of the two mixing components is 20. A careful examination of the time dependence of the fields, correlation functions, and other statistical quantities reveals the following:

1. The velocity field undergoes a complex, nonmontonic evolution both in time and space (Figure 4). The spatially

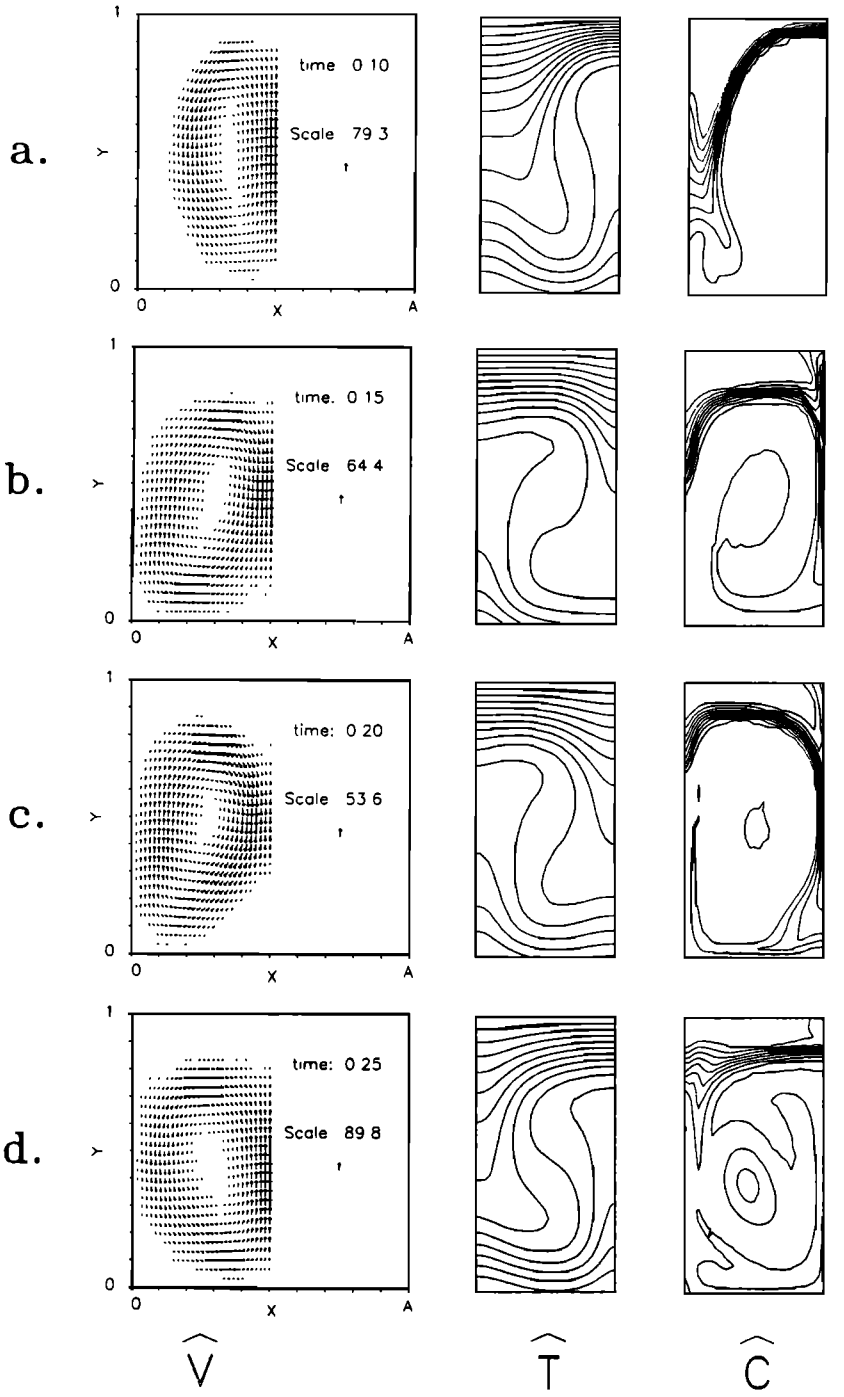

Fig. 4. Velocity ($\hat{V}$), temperature ($\hat{T}$), and composition ($\hat{C}$) at eight times ((*a*) $\hat{t}$ = 0.10, (*b*) 0.15, (*c*) 0.20, (*d*) 0.25, (*e*) 0.30, (*f*) 0.40, (*g*) 0.60, and (*h*) 0.80) during mixing. Dimensionless velocity scale is shown by the vertical arrow in Figures 4*a*–4*h*. In the temperature fields for Figures 4*a*–4*h*, the top of the domain $\hat{y}$ = 1 is at $\hat{T}$ = 0, and the contour interval is 0.04. In the composition fields for Figures 4*a*–4*h*, the contour interval is 0.10 and the highest contours are in the upper part of the domain: (*a*) 0.85, (*b*) 0.85, (*c*) 0.90, (*d*) 0.85, (*e*) 0.90, (*f*) 0.90, (*g*) 0.85, (*h*) 0.56. See text for discussion.

averaged kinetic energy of the flow varies quasi-periodically with peak values during the first half of the mixing event (Figure 6*c*). Velocity reversals are common. For instance, a change from counterclockwise to clockwise circulation occurs between $\hat{t}$ = 0.10 and $\hat{t}$ = 0.15 (cf. Figures 4*a* and 4*b*). The "nucleation" and growth of oppositely circulating vorticies show up very clearly in the kinetic energy plot. The period of the velocity direction reversal is roughly 0.18. For a 5-km-deep chamber, a dimensionless period of 0.18 corresponds to 150,000 years ($t = \hat{t}d^2/\kappa$). An important ramification of the complex evolution of the velocity field is the significance with respect to crystal settling (see below).

2. Comparison of the $\hat{T}$ and $\hat{C}$ fields (Figure 4) shows

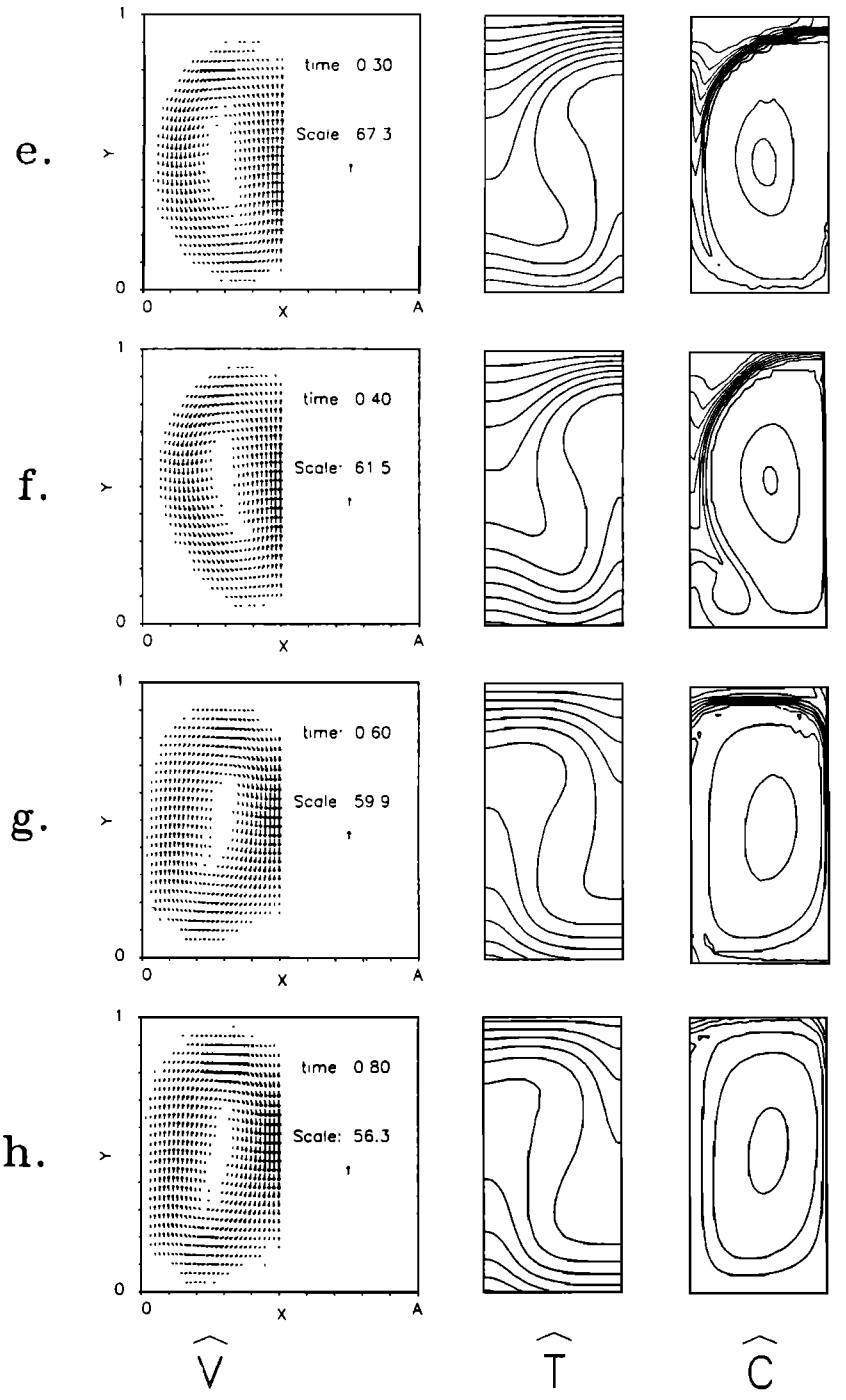

Fig. 4 (continued)

that gradients of the latter are always much steeper. This is a result of the large value of the ratio of thermal to chemical diffusivity utilized in the simulation (i.e., $Le = 200$). For virtually all components in silicate melts at magmatic conditions, $Le > 5000$ [*Trial and Spera*, 1988]. This means that the $\hat{C}$ field will always be much grainier than the corresponding field of $\hat{T}$.

3. The Nusselt number (see (23)), a dimensionless variable that indicates the total heat transport relative to the conductive heat transport, varies quasi-periodically not unlike the averaged kinetic energy (see Figure 6*c*). Note, however, that Nu lags the kinetic energy; this is a consequence of the large Prandtl number of magma which insures that momentum is transported much faster than heat. Because of the nonsteady nature of Nu, the heat flow into the roof of the chamber varies temporally. Note that even at a time corresponding to 40% of the mixing time ($\hat{t}_{mix} = 1.15$), variations in heat flux up to 33% of the value at $\hat{t}_{mix}$ may occur. In the example presented here, minima in Nu occur at $\hat{t} = 0.25$ and 0.45 (Figure 6*c*). Heat flow measurements made at active caldera sites need to be considered in this light.

4. Because advective transport dominates over diffusive transport, the $\hat{C}$ field follows the velocity field closely. Unlike the situation of mixing of a passive component,

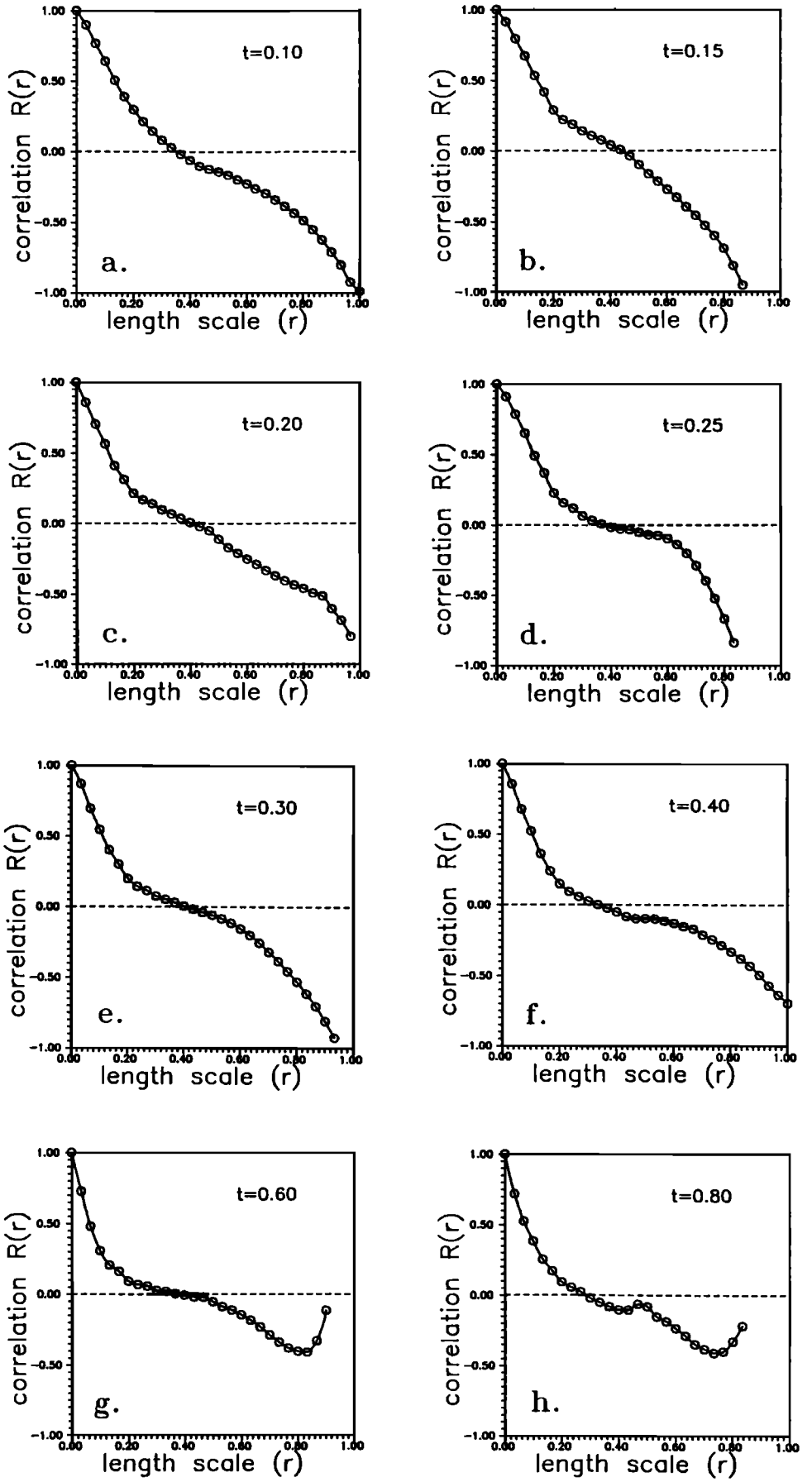

Fig. 5. Correlograms as a function of time for the mixing event depicted in Figure 4. See text for discussion.

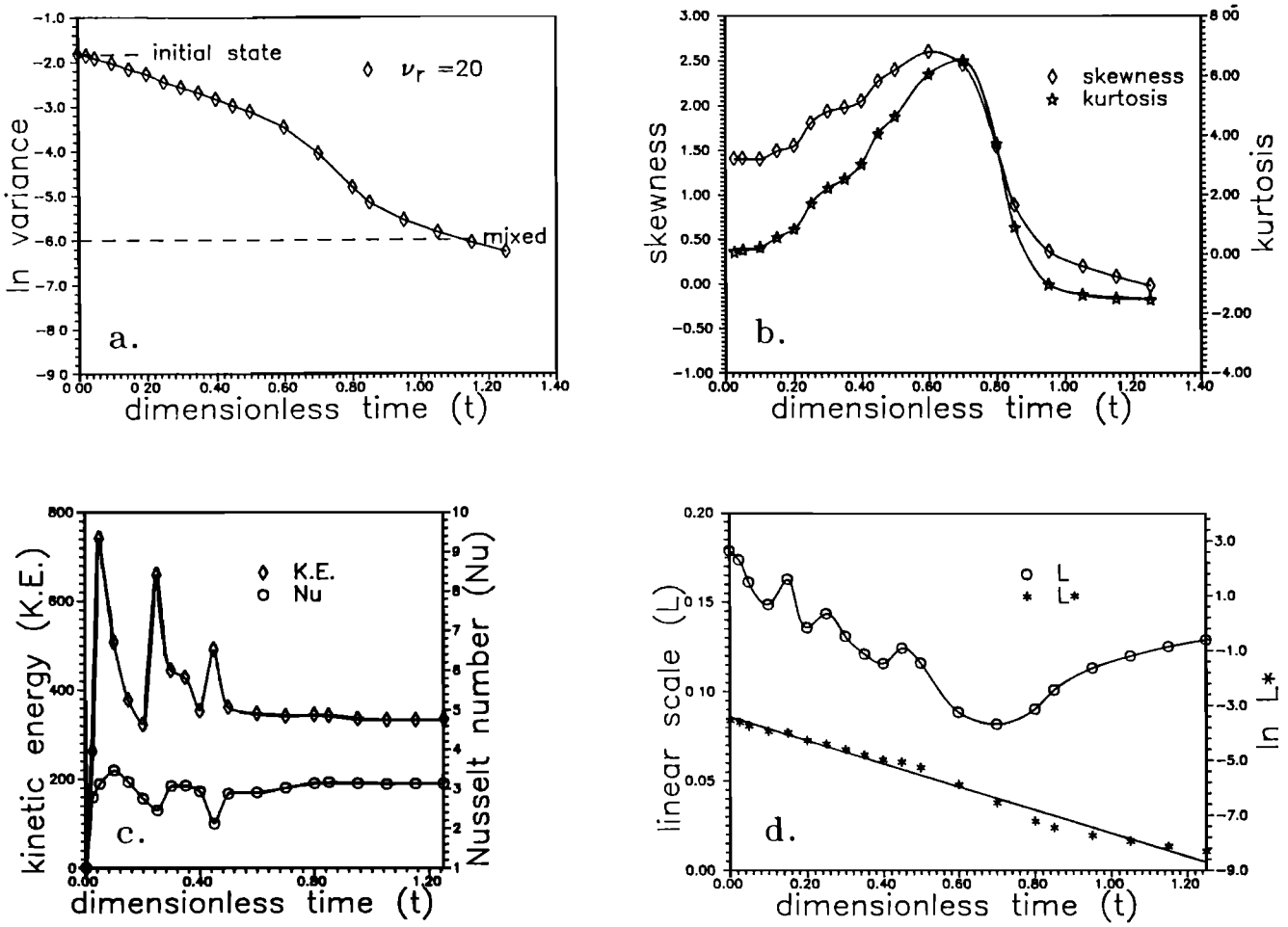

Fig. 6. Statistical moments of composition, kinetic energy and Nusselt numbers, and scales of segregation for the mixing evolution of Figure 4. (*a*) Variance (σ^2) versus time. (*b*) Skewness (m_3) and kurtosis (m_4) versus time. (c) Kinetic energy (defined as $(\hat{U}^2)+(\hat{V}^2)$ integrated over the domain) and Nu , the thermal Nusselt number, versus time. (*d*) The linear (L) and space correlation (L^*) scales versus time. Best fit line for ln L^* versus $\hat{t}$: ln L^* = (-4.23 ± 0.14) $\hat{t}$ - (3.43 ± 0.09) (one sigma).

instabilities within the compositionally buoyant heterogeneities can lead to secondary cells which grow to cause periodic reversals of the flow direction. This effect becomes increasingly important as Rr becomes large.

5. The evolution of the quantity $R(r)$ provides critical information regarding the spatial scale of correlation of the compositional anomalies. The initial $R(r)$ distribution is shown in Figure 2. At early times the $R(r)$ curve is sigmoidal; a significant amount of short range (small r) correlation ($R \approx 1$) and long range (large r) anticorrelation ($R \approx -1$) exists. These correlations are inherited from the initial $\hat{C}$ distribution. As the system evolves, the degree of correlation decreases for pairs with separations in the short to intermediate range. At $\hat{t} = 0.4$ for example (Figure 5*f*), a nearly random space correlation exists for pairs in the range $0.2 < r < 0.65$. At a time corresponding to the mixing time ($\hat{t}_{mix} \approx 1.15$), very little correlation remains for pairs separated by more than 0.2 in dimensionless distance. Because of the destruction of the buoyant top layer, little of the excellent anticorrelation at large r remains. Note the variation in r_o, where r_o is defined as the separation distance at which the compositional spatial correlation is random (i.e., $R(r_o) = R^*(r_o) = 0$), in the sequence of correlograms shown in Figures 5*a*–5*h*.

6. The integral of the space correlation (L^*) and the related parameter L, the linear scale of segregation, provide useful information regarding the size distribution of the compositional anomalies (Figure 6*d*). L^* decays exponentially with time as normal and shear strains reduce the size (or wavelength) of entrained silicic melt. The e-folding time of this process is about 0.25 of a thermal diffusion time unit. The linear scale of segregation (L) decreases from $L \approx 0.2$, a value that reflects the initial thickness of the silicic layer to a minimum value of $L \approx 0.08$ at $\hat{t} \approx 0.7$. Note that the decay of L is not monotonic; times of minima in the L versus $\hat{t}$ relation generally correspond to minima in the kinetic energy function (Figure 6*c*). An important point is that because of the separation of time scales for momentum, heat, and chemical transport, damped oscillations of the velocity field provide a mechanism for temporally local unmixing events. For instance, between $\hat{t} = 0.1$ and $\hat{t} = 0.2$ (Figures 4*a*–4*c*) the linear scale of segregation actually increases! Superimposed on this oscillatory behavior in L-$\hat{t}$ space is an overall decrease in L until $\hat{t} = 0.7$. At that time the average "clump" size (i.e., L) has been reduced to a chemical diffusive length scale $\hat{\delta} \sim (\hat{t}/Le)^{1/2}$. The precise value of L at large times arises through competition between the rate of clump size reduction

through the action of convectively driven strain and the irreversible production of entropy due to chemical diffusion. The former process is measured by dL^*/dt and the latter by the evolution of σ^2. Note that the second law of thermodynamics implies that $\sigma^2 \to 0$ as $t \to \infty$.

7. The evolution of the variance (σ^2), skewness (m_3), and kurtosis (m_4) of the composition field is shown in Figures 6*a*–6*b*. These moments provide quantitative information regarding the intensity of segregation. If chemical diffusion were negligible on all spatial scales at all times, then a frequency-composition plot would be invariant; at any time, 20% of the compositions would be $\hat{C} = 1$ and the remaining would be $C = 0$. The moments σ^2, m_3, and m_4 would consequently remain invariant. Because of the effects of chemical diffusion, however, this is not the case. It is important to note that chemical diffusion is always important at some length scale. As shown in a later section (role of Lewis number), an asymptotic relationship exists between $\hat{t}_{mix}$ and Le which enables one to extrapolate low Le simulations to realistic magmatic situations.

As shown on Figure 6*a*, the logarithm of the variance shows a nonlinear dependence on $\hat{t}$ during mixing. In particular, note the sudden change in rate of decrease of the variance at $\hat{t} = 0.7$. The change in $d \ln \sigma^2/d\hat{t}$ at $\hat{t} = 0.7$ is a reflection of the fact that the maximum pair separation distance (r) over which a reasonably good spatial correlation exists (e.g., $R > 0.5$, say) is approximately equal to the diffusive length scale defined according to

$$\hat{\delta} = \frac{\delta}{d} = (\hat{t}/Le)^{1/2} \qquad (26)$$

That is, from Figures 5*g* and 5*h*, note that $R(0.06) \approx 0.5$ at $\hat{t} \approx 0.6$. If one identifies r with $\hat{\delta}$ in (26), then one finds $\hat{t} = 0.6$ for the time at which the characteristic correlation length equals the diffusive length scale for the Lewis number of this experiment ($Le = 200$). Recall that the linear scale of segregation (L) also attains a minimum value at $\hat{t} = 0.7$.

Finally, one may examine the evolution of the skewness and the kurtosis of the composition-frequency relationship. Recall that the skewness characterizes the degree of asymmetry of a distribution about its mean such that positive values signify asymmetric tails extending out toward more silicic compositions and negative values signify tails extending out toward more mafic compositions. From Figure 6*b*, note that $m_3 > 0$ for virtually all of the mixing history, reflecting the asymmetric distribution of $\hat{C}$ values extending toward silicic compositions. Significantly, the skewness attains a maximum value ($m_3 \approx 2.5$) at $\hat{t} = 0.7$ and thereafter eventually decreases toward zero (i.e., toward a symmetric frequency-composition distribution). The significance of the maximum m_3 value is that for all $\hat{t} < 0.7$, some nearly pure silicic melt (say, $0.9 < \hat{C} < 1$) still may be found within the chamber. At times greater than that at which $dm_3/d\hat{t} = 0$, essentially all of the silicic melt has been contaminated by mafic melt. For $\hat{t} > 0.7$, the highest $\hat{C}$ value found anywhere within the chamber quickly falls, and as a consequence, the frequency-composition histogram (not shown) becomes increasingly symmetric. A nearly perfectly mixed fluid has a symmetric (Gaussian) frequency-composition distribution.

The kurtosis (m_4) measures the relative peakedness ($m_4 > 0$) or flatness ($m_4 < 0$) of the frequency distribution of compositions and is also plotted in Figure 6*b*. Recall that the kurtosis of a normal distribution is zero. Note that like the skewness, the kurtosis increases until a maximum is attained at $\hat{t} = 0.7$ ($m_4 = 6.5$). Thereafter, m_4 decreases systematically until values indicative of a normal or near-normal distribution are attained.

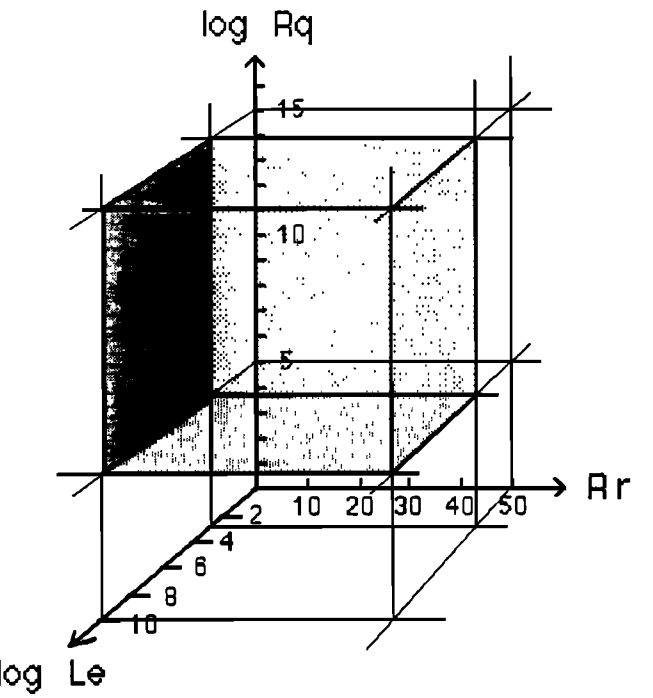

Fig. 7. The domain of crustal magma bodies in Rq, Rr, and Le parameter space. Numerical simulations are at present restricted, for practical reasons, to a region in the rear, lower left of the cube.

Parameter Study

In order to investigate how the rate of magma mixing depends on the properties of magma and the shape of the magma body for one particular set of initial and boundary conditions, we have made a systematic numerical study of the dependence of $\hat{t}_{mix}$ on the parameters of the problem including effects of viscosity contrast. We present simulations for magma mixing with Rq between 10^5 and 3 x 10^5, Rr between 0 and 1.1, aspect ratio (A) between 0.3 and 3, and viscosity ratios (ν_r) from 1 to 20. Limitations on CPU time generally restrict the ranges of parameters to values only partially appropriate for natural systems. In Figure 7 the approximate limits on Rq, Rr and Le appropriate to magmatic systems are shown [eg., *Clark et al.*, 1987]. Recall also that the spatial resolution of the simulations is between 1/30 and 1/60 of the chamber dimension (d). The results of the numerical simulations presented here are only a first step to identify first-order trends and effects of the parameters and boundary conditions on the convective mixing dynamics of magmatic systems.

In all of the simulations with $Rr < 1$ and the linear initial condition on $\hat{T}$ (condition (25*c*)), mixing begins immediately with a convective overturn. However, near the interface, the upper layer is less dense than the fluid immediately below it for any $Rr > 0$. This creates a locally stable density profile near the interface between the upper

and lower layers. Thus there is a global instability which drives convection while local stability resists motion for any Rr between zero and one. The system is very sensitive to Rr, and even small amounts of compositional buoyancy (e.g., $Rr = 0.1$) cause fundamentally different mixing dynamics from passive mixing even though the overall initial density distribution is only slightly different. Simulations employing the step-$\hat{T}$ initial condition (condition (25*b*)) mix in about one half the time of the linear $\hat{T}$ cases for $Rr < 1$ due to the thermally induced density instability at the interface. Simulations employing a constant temperature initial condition ($\hat{T} = 0$) mix about 5 times more slowly, since the initial state is stable for any $Rr \geq 0$.

A double-diffusive convection simulation can be portrayed by plotting velocity, temperature, and composition at successive times. The mixing process can be more compactly presented by plotting the variance and scale of segregation versus time and, subsequently, $\hat{t}_{mix}$ versus the parameter of interest. The variance and scale of segregation are calculated with compositions from a fixed number (961) of equidistant points independent of the number of nodes used in any simulation and approximately equal to the number of nodes in the coarsest discretization (841). Where the aspect ratio is not equal to 1, the number of points used to calculate the variance and scale of segregation is adjusted so that the point density is equal to the point density when $A = 1$. In this way, the variances and scales of segregation are comparable regardless of the number of nodes used in the simulation and the aspect ratio of the domain. We consider next the effects of Le, Rr, Rq, viscosity ratio (ν_r), and aspect ratio (A) in turn.

Role of Lewis Number

In the absence of convection, the present mixing problem reduces to a diffusional mixing process, and the Lewis number ($Le = \kappa/D$) controls how quickly homogenization takes place. From simple diffusion theory, the effective mixing time is $t_{mix} \sim Led^2/\kappa$, which is far greater than characteristic solidification times and hence too long to be relevant to magma bodies. However, we are interested in convective mixing where both the effects of diffusion and deformation are important. In order to quantify the effect of diffusion on convective mixing, the functional dependence of Le on $\hat{t}_{mix}$ and the temporal evolution of the linear and volume scales of segregation have been investigated.

The mixing time $\hat{t}_{mix}$ increases as Le increases for convective mixing for $Rq = 10^5$, $Rr = 0.25$, and $\nu_r = 1$ (constant viscosity) (Figure 8*a*). A similar functional relationship (not plotted) was found at $Rq = 2 \times 10^5$, $Rr = 0.25$, and $\nu_r = 1$ (constant viscosity), except the mixing times were shorter (by a factor of 1.3) due to enhanced deformational mixing. Similarly, at $Rq = 3 \times 10^5$, mixing times were shorter than the $Rq = 10^5$ case by a factor of about 3. More on the Rq dependence of $\hat{t}_{mix}$ is given later. Plotted in Figure 8*b* is the linear scale of segregation (L) versus time. The linear scale (L) decreases sharply at early times ($\hat{t} = 0$ to 0.025) because convection has begun to entrain the upper layer and there has not been time for appreciable diffusion. A reversal in the direction of flow after $\hat{t} = 0.025$ causes an increase in L between $\hat{t} = 0.025$ and $\hat{t} = 0.05$. This increase in L is an effective unmixing phenomenon caused by a reversal in the sense of rotation of the fluid. Although velocity unsteadiness has been observed in some time-dependent thermal convection simulations [e.g., *Jarvis*, 1984], inclusion of compositional buoyancy clearly produces the new effect of reversals in the velocity field. The ratio L/V generally increases with Le reflecting the greater elongation of the compositional anomalies (i.e., the clumps), which is possible when chemical diffusion is slower (Figure 8*c*). In Figure 8*d*, $\hat{t}_{mix}$ versus Le is shown. The mixing time increases as a power law function of Le according to

$$\hat{t}_{mix} = 0.027(Le)^{0.45} \tag{27}$$

Approximate estimates of $\hat{t}_{mix}$ at geologically relevant Le ($5000 < Le < 10^{10}$) can be made from the relationship plotted in Figure 8*d*. Clearly, large Le slows convective mixing by increasing the time required by the action of shear and normal strain effects to reduce the size of a compositional anomaly to a diffusive one. Note that the parameters chosen ($Rq = 10^5$, $Rr = 0.25$) correspond to a weakly convecting (low Rayleigh number) magma body. At the low range of typical Le, say, $Le = 5000$ (see *Clark et al.* [1987] and *Trial and Spera* [1988] for discussion of D values and multicomponent chemical transport), $\hat{t}_{mix} \approx 1.3$. Since the dimensional time is given by $t = d^2\hat{t}/\kappa$, the mixing time in this case is close to the conductive time scale. At higher and more typical Le, say, $Le = 10^6$, $\hat{t}_{mix} \approx 13.5$.

Role of Compositional Buoyancy

The initial condition in the model has viscous silicic magma above a less viscous mafic magma. The difference in density arising solely from the effects of composition is given by $\Delta\rho = \rho_0\beta\Delta C$, where ΔC is the difference in composition between pure "light" and pure "heavy" component. The parameter Rr represents the ratio of chemical to thermal buoyancy and hence is a measure of the importance of chemical buoyancy. One may easily study the dispersion of a passive tracer by setting $Rr = 0$ and solving for the $\hat{C}$ field. A low-concentration minor, trace, or rare Earth element (REE) behaves dynamically as a passive contaminant. The more interesting case of nonzero Rr is of greater interest to petrologists due to the wide variation in the density of naturally occurring melts at similar temperatures. Recall that Rr may be large for natural magmas (Figure 7). As a first step toward understanding the role of compositional buoyancy in convective mixing, we have varied Rr systematically from small values to larger values. It is important to note that $\hat{t}_{mix}$ is a complicated function of both Rr and the thermal Rayleigh number Rq.

The mixing time is plotted versus Rr for three values of Rq in Figure 9*a*. There are three important conclusions which may be drawn from this figure. First, for a given value of Rr, increasing Rq always decreases the mixing time. For example, at $Rr = 0$ and $Rr = 0.5$ the mixing times at $Rq = 3 \times 10^5$ are roughly 6 and 3 times shorter, respectively, than at $Rq = 1 \times 10^5$. Second, the Rr at which the mixing time is a minimum shifts to lower values as Rq increases. Observe

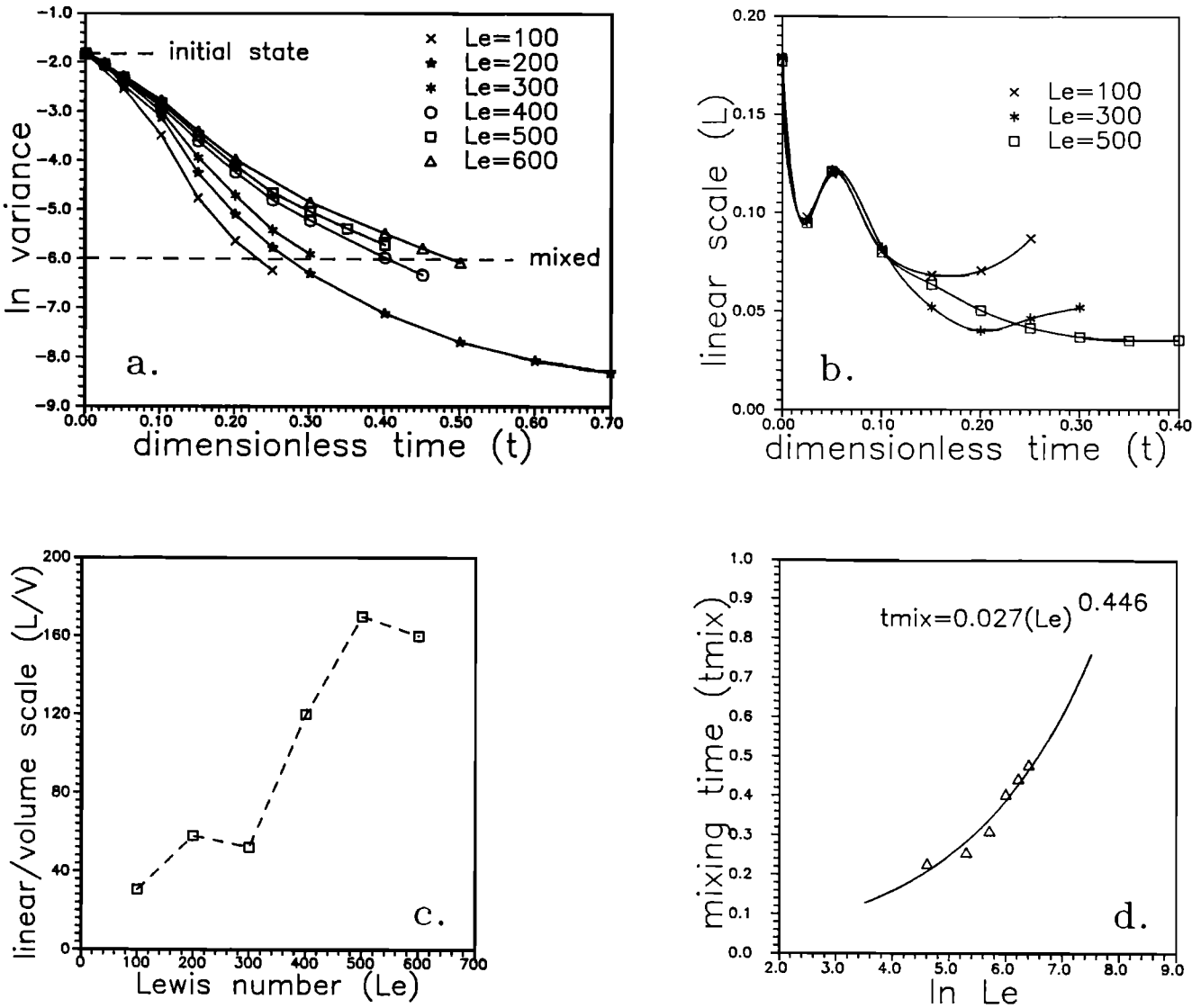

Fig. 8. Lewis number effects on mixing. (*a*) Variance (σ^2) versus time for six values of *Le*. The mixing time is larger at larger *Le*. (*b*) Linear scale (*L*) versus time for three representative values of *Le*. Diffusion begins to dominate over advection in mixing at larger scales and at shorter times for small *Le* as indicated by the locations of the local minima in *L* versus $\hat{t}$. (*c*) Ratio of linear to volume scales versus *Le* at $\hat{t} = \hat{t}_{mix}$. Heterogeneities are more elongated during mixing at larger *Le*. (*d*) Mixing time versus *Le*. The mixing time increases as a power law function of *Le*: $\ln \hat{t}_{mix} = (0.446 \pm 0.058) \ln Le - (3.62 \pm 0.33)$ (one sigma).

that at $Rq > 3 \times 10^5$, the minimum mixing time would likely occur at $Rr = 0$ (passive mixing) as one might expect. At lower Rq, however, a minimum mixing time occurs at a small positive Rr value (e.g., at $Rq = 1 \times 10^5$, the minimum mixing time occurs at $Rr \approx 0.25$).

A possible explanation for this behavior is as follows. Deformation occurs when velocity gradients in the convecting fluid cause normal and shear strain in the heterogeneities. If the heterogeneitites are dynamically active, not passive, their composition gives rise to localized buoyancy forces superimposed on the large-scale thermally driven circulation. The net effect of this superposition is to increase vorticity in the neighborhood of the heterogeneity and thereby locally enhance shear deformation. A small difference in buoyancy between two mixing fluids enhances convective mixing at low Rq. If Rr is sufficiently large, however, the initial condition, that of a stable configuration of light fluid above dense fluid, overwhelms the effect of local vorticity on the mixing process.

The final point relevant to Figure 9*a* is that the mixing time varies according to Rq^{-1}, approximately. It is important to note that this conclusion is based on a limited range of Rq values and needs to be addressed further. At face value, an extrapolation based on the present data suggests that, for example, $\hat{t}_{mix} \sim 0.03$ for $Rq = 3 \times 10^6$ at $Rr = 0.5$. Note from Figure 9*a*, $\hat{t}_{mix} = 0.3$ for $Rq = 3 \times 10^5$ at $Rr = 0.5$.

The fundamental difference between passive ($Rr = 0$) and dynamic ($Rr \neq 0$) mixing can be seen in Figure 9*b*, where L/V is plotted versus $\hat{t}$ for $Rq = 10^5$. In passive mixing, the ratio L/V decreases steadily after an initial increase associated with the onset of convective mixing. This steady decrease in L/V was observed at all values of Rq. In the case of dynamic mixing, flow reversals and unmixing caused by compositional buoyancy occur. These flow reversals are seen

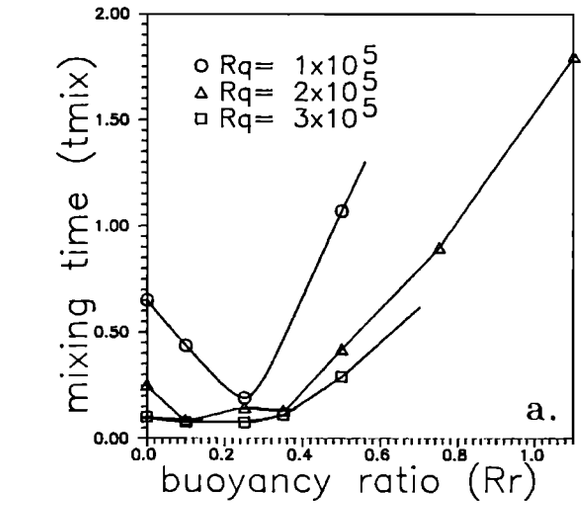

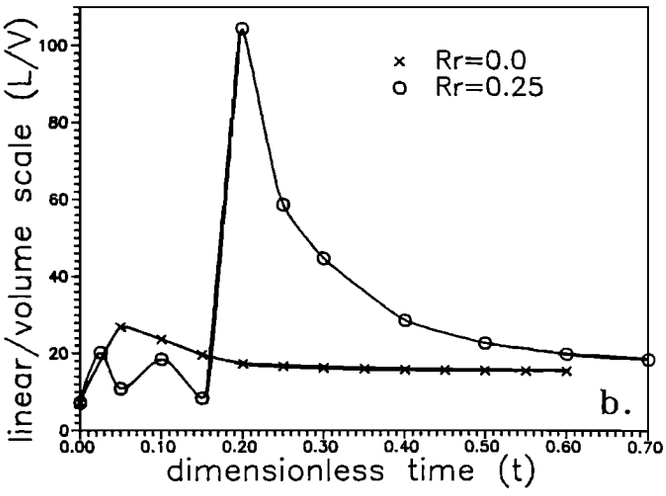

Fig. 9. Compositional buoyancy effects on mixing. (*a*) Mixing time ($\hat{t}_{mix}$) versus *Rr* for three values of *Rq*. Mixing times are smaller for larger *Rq*. At fixed *Rq*, $\hat{t}_{mix}$ is larger for *Rr* = 0 (passive mixing) than for *Rr* < 0.30. However, the *Rr* at which this minimum in $\hat{t}_{mix}$ occurs approaches *Rr* = 0 as *Rq* increases. Note that the mixing criterion for this plot only was chosen to be σ = 0.08 instead of σ = 0.05. (*b*) Ratio of linear to volume scale versus time for passive (*Rr* = 0) and dynamic (*Rr* = 0.25) mixing with $Rq = 10^5$, *Le* = 200, $\nu_r = 1$, *A* = 1. In passive mixing, there are no flow reversals and *L/V* decreases monotonically from a maximum near the beginning. In dynamic mixing, flow reversals and the associated unmixing phenomena cause *L/V* to oscillate until about $\hat{t}_{mix}$ when the intensity of the heterogeneity is too low to cause flow reversals.

as oscillations in *L/V* versus $\hat{t}$ and occur at all values of *Rq* studied. Such flow reversals are a fundamental feature of double-diffusive convection and have significant consequences for the evolution of magma bodies.

Role of Variable Viscosity

In considering the mixing of magmas, one must take into account the difference in viscosity of the two mixing components. A detailed description of the mixing process for a system with a viscosity contrast of 20 was presented in Figures 4, 5, and 6. In Figure 10*a* the variance (σ^2) is plotted versus time for viscosity ratios of 1, 2, 10, and 20 with *Rq* = 2 x 10^5, *Rr* = 0.25, *Le* = 200, and *A* = 1. The mixing time ($\hat{t}_{mix}$) increases as the viscosity contrast increases (Figure 10*b*) according to the power law expression

$$\hat{t}_{mix} = 0.023(\nu_r)^{0.524} \tag{28}$$

For example, a viscosity contrast of 10^3 implies $\hat{t}_{mix} \approx 8$ at *Rq* = 2 x 10^5, *Rr* = 0.25, and *Le* = 200, which is about 35

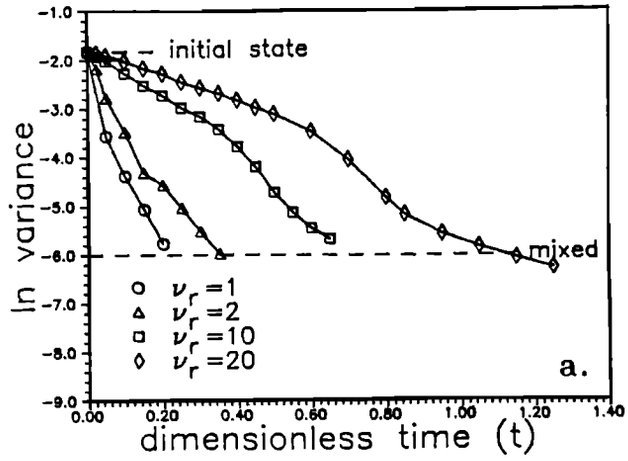

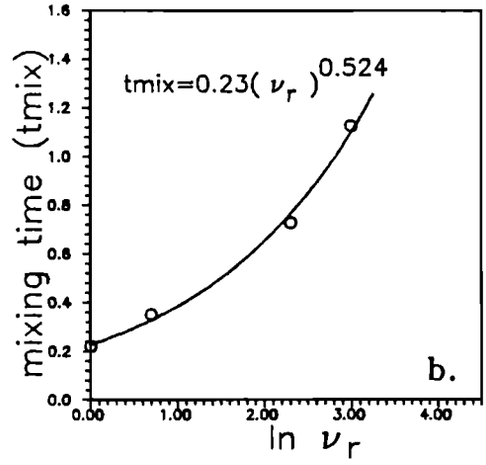

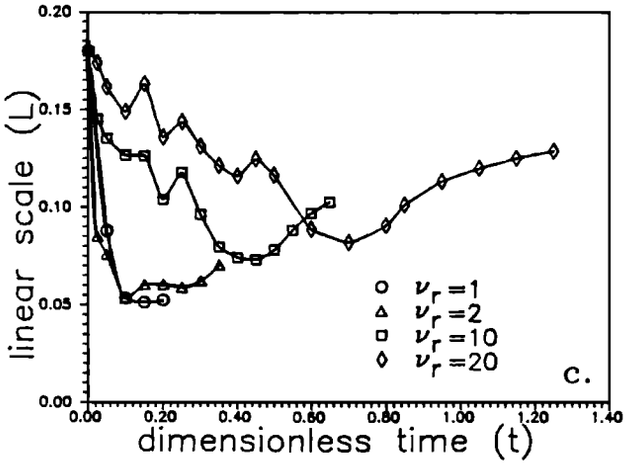

Fig. 10. Viscosity effects on mixing. (*a*) Variance (σ^2) versus time for four viscosity ratios with *Rq* = 2 x 10^5, *Rr* = 0.25, *Le* = 200, and *A* = 1. (*b*) Mixing time $\hat{t}_{mix}$ versus ν_r for the same parameters as in Figure 10*a*. Mixing time increases as a power law function of ν_r: $\hat{t}_{mix} = 0.23\ \nu_r^{0.524}$. One-sigma errors are as follows: $\ln \hat{t}_{mix} = (0.524 \pm 0.025) \ln \nu_r - (1.47 \pm 0.048)$. (*c*) Linear scale (*L*) versus time for four viscosity ratios. The linear scale is larger just prior to $\hat{t}_{mix}$ for larger ν_r, reflecting the difficulty of deforming more viscous heterogeneities.

times slower than the constant viscosity case. The linear scale (L) versus time is shown in Figure 10*c* for the four viscosity ratios. The nonmonotonic nature of the evolution of L is due to the velocity reversal phenomenon discussed in detail earlier for the case $\gamma_r = 20$. Similar behavior causes the wiggles in L versus t for the other viscosity ratios. Generally, L is large for high-viscosity contrasts because of the tendency for high-viscosity compositional anomalies to resist deformation. These results suggest that large viscosity differences within magma bodies (e.g., rhyolitic cap and basaltic interior) can be preserved for periods corresponding to many times the characteristic thermal diffusion time d^2/κ. In a closed system, this implies that the effects of crystallization, with concomitant increase in viscosity and a drop in Rq, would overwhelm the effects of convective mixing. Large Sierran-type plutons which often exhibit diverse patterns of vertical and/or radial zonation may be examples of low Rq systems which mix only incompletely before the "rheological locking temperature" (defined by *Furman and Spera* [1985]) is attained.

Role of Magma Body Shape

The effect of magma body aspect ratio ($A = w/d$) on the mixing process was investigated by carrying out a number of simulations applicable to domains ranging from slot or dikelike bodies ($A = 0.3$) to sheet or sill-like bodies ($A = 3$).

An important conclusion of this study is that the mixing is strongly dependent on aspect ratio; mixing is most efficient in roughly equant ($A = 1$) magma bodies. Figure 11*a* shows this effect rather dramatically for fixed parameters, $Rq = 3 \times 10^5$, $Rr = 0.10$, $Le = 200$, and $\nu_r = 1$. Note that the optimally shaped body ($A \approx 1$) mixes at time $\hat{t}_{mix} = 0.10$, whereas a body that is twice as deep as it is wide ($A = 0.5$) requires $\hat{t}_{mix} = 0.17$ and a body that is 3 times as wide as it is deep ($A = 3$) requires $\hat{t}_{mix} = 1.4$. Clearly, the shape of a magma body exerts a major influence on its mixing history for $A \geq 2$ and $A \leq 1/2$. For dikelike bodies ($A < 1$), $\hat{t}_{mix}$ is relatively large because of the presence of constricting walls. The overall strain rates associated with reduced convective velocities are not as effective in entraining and mixing the upper layer. In sill-like bodies ($A > 1$), multiple convection cells form in the horizontal direction (Figure 11*b*) with the effect of substantially increasing the mixing time. This occurs because although each convection cell is individually well mixed, compositional differences among the cells can persist.

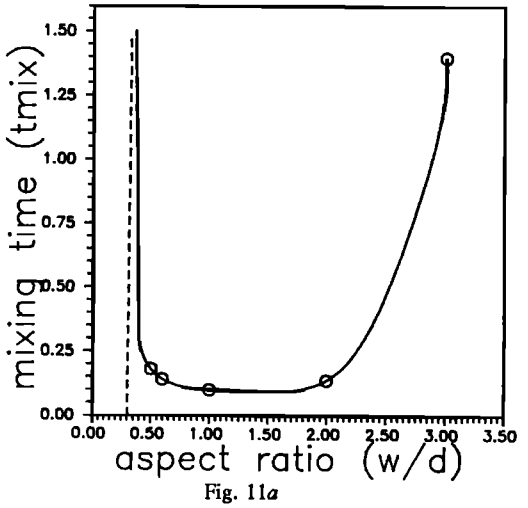

Fig. 11*a*

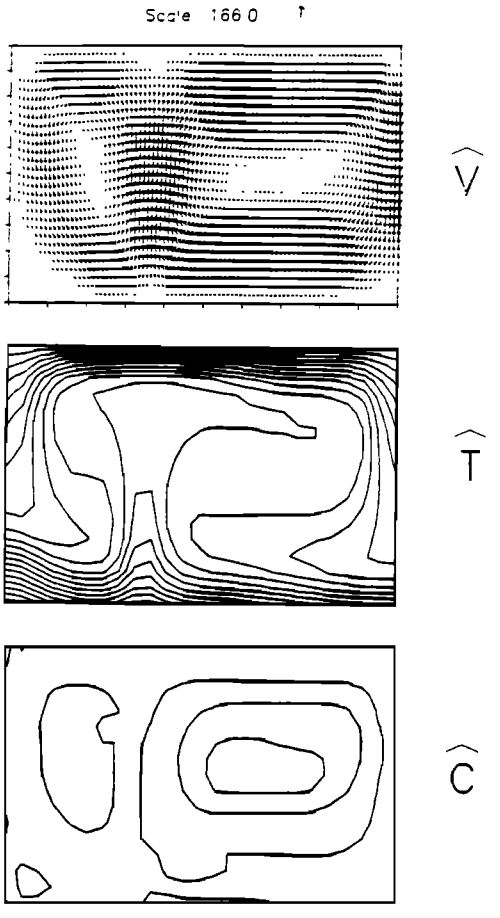

Fig. 11*b*

Fig. 11. Aspect ratio effects on mixing. (*a*) Mixing time ($\hat{t}_{mix}$) versus aspect ratio ($A = w/d$) shows the strong dependence of $\hat{t}_{mix}$ on shape with $Rq = 3 \times 10^5$, $Rr = 0.10$, $Le = 200$, and $\nu_r = 1$. For both sill-like ($A > 1$) and dikelike ($A < 1$) shapes, the mixing time is relatively long, while equant shapes mix most quickly. Bodies with $A \leq 0.30$ have conductive solutions at these parameter values and mix by diffusion only. See text for discussion. (*b*) Velocity, temperature, and composition fields for the sill-like body ($A = 3$) at $\hat{t} = 0.20$. Two cells with different compositions form laterally across the chamber. Note that a vertical compositional gradient has been transformed into a lateral compositional gradient by purely convective means. Velocity scale is given by vertical arrow. Contour interval for $\hat{T}$ is 0.02, and the top of the domain is at $\hat{T} = 0$. Contour interval for $\hat{C}$ is 0.1, and the subelliptical contour in the right-hand cell is $\hat{C} = 0.04$.

Other Thermal Boundary Conditions

Four additional thermal boundary conditions have been investigated: (1) time-dependent heating from below with constant temperature at the roof, (2) cooling out the sidewall with heating from below and constant temperature at the roof, (3) cooling out roof, sidewall, and floor, and (4) cooling out the roof only. Plotted in Figure 12 is $\ln \sigma^2$ versus time for these four conditions, and each is discussed, in turn, below.

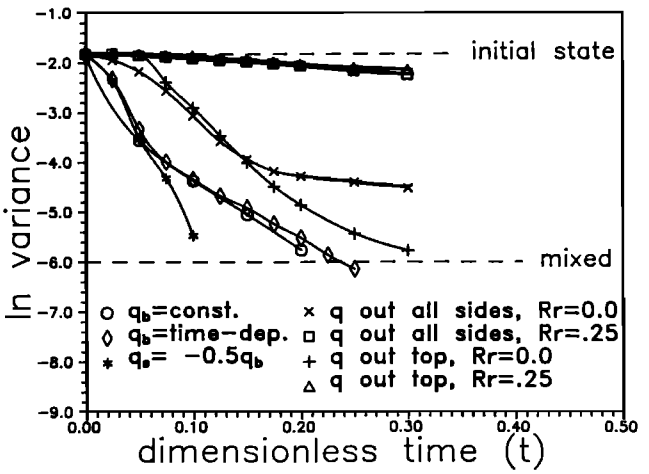

Fig. 12. Variance (σ^2) versus time for five different boundary conditions. In all cases, $Rq = 2 \times 10^5$, $Rr = 0.25$, $Le = 200$, $A = 1$, constant viscosity, unless otherwise stated. For the cooling out the top and cooling out all boundaries cases, the initial temperature is constant in the domain. For the constant q_b, time-dependent q_b, and q_w cases, the initial temperature decreases linearly from bottom to top. Note the similarity in evolution between the case where there is cooling out the top and cooling out all sides for $Rr = 0.0$ and $Rr = 0.25$. Note also the similarity between the case where there is constant heat flux and where it is time dependent ($q = q_b$ $(-2.24\hat{t}^{1/2} + 1)$).

To simulate the time-dependent heating caused by an influx of hotter magma into the magma body, a heat flux proportional to the square root of time was specified at the floor. The function chosen ($q = q_b(-2.24\ \hat{t}^{1/2} + 1)$) requires the heat flux to decay from its maximum at $\hat{t} = 0$ to zero at $\hat{t} = 0.2$ and then become negative at subsequent times (i.e., cooling out the floor). The sidewall is taken to be adiabatic, and the roof is held at a constant temperature. The initial conditions are identical to that of the constant flux scenario (i.e., linear $\hat{T}$, and step $\hat{C}$). The curve in Figure 12 shows that the mixing time and style with time-dependent heat flux are almost identical to the constant heat flux case.

Cooling out the lateral margins causes the mixing to occur in about one-half the time of the adiabatic sidewall case, a not unexpected result. The cooling in the case shown in Figure 12 is specified as a constant flux equal in magnitude to one-half the flux entering the body along the floor ($q_w = -0.5q_b$). The initial conditions are linear $\hat{T}$ and step $\hat{C}$. Simulations with various degrees of sidewall cooling show that mixing times approach an apparent asymptotic value ($\hat{t}_{mix} = 0.11$ as the cooling increases from zero to the maximum ($q_w = -0.5q_b$). For $Rr = 0.25$, flow reversals do not occur for $-q_w > 0.3q_b$, although for higher Rr, flow reversals would likely occur at larger q_w.

Thermally disconnected magma bodies were simulated by specifying a constant heat flux out the roof, sidewall, and floor. The initial condition employs step $\hat{C}$ and constant $\hat{T}$ (hot) everywhere in the body. The curves for $Rr = 0$ and $R = 0.25$ are shown for this case in Figure 12. For passive mixing ($Rr = 0$) there are no flow reversals, and mixing proceeds at a rather slow rate. For dynamic mixing ($Rr = 0.25$), convection is also undirectional with mixing very slow. Convection occurs for both cases ($Rr = 0$ and $Rr = 0.25$), but the rates of mixing are slow relative to the standard heating from below scenario because of the gravitational stability of the initial state and because the entrainment of silicic melt by convecting mafic melt which occurs in the heating from below scenario is very limited when cooling occurs from all sides.

A case in which cooling occurs only out the roof is also presented in Figure 12. The boundary condition at the roof specifies a constant flux of heat out; initial conditions are as in the previous case. Again, curves for $Rr = 0$ and $Rr = 0.25$ are shown. The passive case ($Rr = 0$) mixes relatively well, circulating in one direction, while the dynamic case ($Rr = 0.25$) mixes very slowly, with flow reversals common. The strong dependence of Rr arises in this and the previous scenario because the thermal instabilities which drive the flow must occur largely in the compositionally buoyant layer. This is different from the standard case in which entrainment by the convecting lower layer contributes to the mixing. The mixing time for the $Rr = 0.25$ case is almost identical to that in the cooling from all sides scenario.

CONCLUSIONS AND PETROLOGIC IMPLICATIONS

The scale and intensity of segregation are general measures of the goodness of mixing. With sufficient exposure and geochemical data, these two quantities can be determined, and the degree of mixing of lava or pyroclastic flow deposits and plutonic bodies can be evaluated and compared. If the intensity of segregation is near the analytic uncertainty of the measurement of composition, hybridization has occurred, and additional evidence for mixing should be sought at smaller scales (e.g., phenocryst disequilibrium or cryptic hybridization as defined by *Dungan* [1987]). If the intensity is large (i.e., near 1), commingling has occurred. The linear (or volume) scale of segregation provides important evidence for the kind of commingling process that has occurred and corresponds approximately to the length scale given in Table 1. In numerical simulations of magma mixing, calculations of the scale and intensity of segregation allow one to follow the mixing process through time and to compare the degree of mixing of any two simulations at any time.

Convective magma mixing occurs by complex, time-dependent flows. The mixing time depends nonlinearly on many factors, including heat flux driving convection, the rate of diffusion of chemical species, the relative importance of thermal and chemical buoyancy, the viscosities of the mixing components, and the shape of the magma body. Because relatively small Rayleigh numbers are used in the numerical simulations presented here, the effects of the above factors on mixing times of natural thermally open magmatic systems will only be discussed in general terms. The small chemical diffusivities of chemical species in magma (i.e., large Le) prevent diffusion-related mixing from being a significant process until the sizes of heterogeneities have been reduced, through the action of convectively driven normal and shear strains, to a diffusive scale (typically of order 1 m). According to our results, $\hat{t}_{mix}$ is proportional to $Le^{1/2}$ so that for all other factors fixed, a system with $Le \sim 10^8$ mixes ≈ 700 times slower than one with $Le = 200$. That is, the mixing time is roughly 200 times the thermal conduction time. It is probable that magma cooling and extensive crystallization would occur by this time if the magma body were a closed system. Alternatively, if there is a strong thermal connectivity between the magma body and

its source which persists over time, the conductive time scale is not relevant. Mid-ocean ridge axial magma chambers, oceanic hot spot magma chambers (e.g., Hawaii), and some high volcanic output systems on the continents (e.g., Yellowstone) are thought to be examples of thermally well-connected systems.

The crucial petrologic question is the role of magma replenishment in terms of heat content of the body and its temporal variation and the introduction of chemical heterogeneities by the juxtapositioning magmas of differing compositions. The recent studies by *O'Brien et al.* [1989] provide textural and mineralogical evidence for the repeated bringing together of different magma compositions. Heterogeneous source regions could supply magmas of varying compositions to superjacent magma reservoirs. At low Rq and high Le and Rr these magmas would mix only slowly with time scales larger than conductive scales (e.g., $t_{mix} > 10\ d^2/\kappa$).

Increasing the heat input (i.e., increasing Rq) with all other parameters held constant will cause fluid heterogeneities to attain diffusive length scales more quickly. Mixing in a viscous granitic body in some late stage of crystallization (i.e., small Rq) may be inefficient. The presence of thin schlieren at small (cm to m) scales and radial and vertical zonation at large (km) scales in many granitic (sensu latu) bodies testifies to the inadequate time available for convection and diffusion to hybridize magma prior to solidification. From the limited data available on the Rq dependence of t_{mix} at fixed Le and Rr, it is tentatively concluded that t_{mix} is proportional to Rq^{-1}. This relation is only a guide and is subject to future refinement.

The effect of compositional buoyancy is to increase mixing times and to produce complex convective patterns in space and time, including flow reversals. At large fixed Rayleigh numbers, the mixing time increases as compositional buoyancy becomes more important. However, fast mixing following the inversion by entrainment of very buoyant fluid under less buoyant fluid has also been noted (see Figure 9*a*). The study of *Hansen and Yuen* [1987] has shown the danger of viewing double- (or multi-) diffusive convection in strict terms of either the "diffusive" or "finger" regime in the sense defined by *Turner* [1985]. During any finite amplitude double-diffusive convection process, both regimes operate concurrently. Importantly, the mixing time represents the response of the system to the nonlinear superposition of small-scale "finger" and large-scale "diffusive" instabilities. The distinct and characteristic nonlinear behavior of double-diffusive convection cannot be emphasized enough in the petrologic context both because of the inherent complexity of the governing conservation equations and because of the influence of the initial distributions of composition and temperature on the mixing history. Unfortunately, the initial conditions are usually poorly constrained by observations, although the consequences of specific limiting cases may be studied by forward modeling. Simple but careful petrographic description combined with accurate (and absolute) geological histories relevant to the lava or pyroclastic flow deposit or the plutonic body under investigation are therefore critically important.

Flow reversals (see Figures 4 and 9*b*) with concomitant short periods of magma unmixing are intrinsic to double-diffusive convection and may have some significant petrological ramifications. For example, models of crystal settling employing either steady state or simple transient flows [e.g., *Marsh and Maxey*, 1985; *Weinstein et al.*, 1987] are not entirely applicable to double-diffusive systems. Similarly, the variation in the heat flux supplied to the roof of the magma chamber (Figure 6*c*) can be significant through time. Heat flow measurements made at active caldera sites need to be considered in this light. Furthermore, distinct periods of extensive hydrothermal alteration may correspond to times of peak heat transport (i.e., maximum Nu). Based on our limited results, it appears that t_{mix} is proportional to Rr^2 for Rr values greater than about 0.35. This result is consistent with the earlier mean field results of *Clark et al.* [1987] and the two-dimensional simulations of Hansen and Yuen [*Hansen and Yuen*, 1987].

A viscosity contrast between the upper buoyant silicic layer and the lower, mafic one will increase the mixing time approximately according to $\nu_r^{1/2}$. For example, for all other parameters constant the mixing time is 100 times longer for mixing of a 10^5 Pa s silicic melt lying above a 10 Pa s basaltic one compared with the isoviscous case. Of course it should be noted that although silicic melts are always more viscous than mafic ones at the same temperature, the solidi and liquidi are substantially different for silicic and mafic magmas, and the effects of magma crystallinity on viscosity will dominate over compositional effects at temperatures near the solidi. A more complete discussion of this effect is presented by *Sparks and Marshall* [1986] and *Frost and Mahood* [1987].

The shape of the magma body exerts a fundamental control on the rate of mixing. Earlier studies by *Shaw* [1965] in a geological context and *Lighthill* [1953] in a fluid dynamic one clearly point out the sensitivity of the circulation pattern on aspect ratio ($A = w/d$). In double-diffusive convection this effect is even more extreme (Figure 11*a*). In tall, narrow chambers ($A < 1$), mixing in the vertical is greatly inhibited by the presence of walls, and the vigor of convection decreases rapidly. For $A < 1/3$ (approximately), even a weak initial chemical stratification is sufficient to practically stagnate a flow, at least for Rq in the range $10^5 < Rq < 3 \times 10^5$.

In shallow, wide chambers ($A > 1$), multiple convection cells form in the horizontal. Significantly, the rate of chemical exchange between the cells is small. Consequently, cells are of distinct composition and remain so for times far greater than the characteristic cooling time of the magma body ($\sim d^2/\kappa$). Note furthermore that even for $A > 2$, which is not an extreme state of affairs, this phenomenon may be found. Research carried out in recent years on the dynamics of magma withdrawal [*Blake*, 1981; *Spera*, 1984; *Blake and Ivey*, 1986*a*, *b*; *Spera et al.*, 1986; *Freundt and Tait*, 1986] has clearly shown that magma arrives at the bottom entrance of the conduit simultaneously from a region of finite extent in both the horizontal and vertical directions (e.g., Figure 1 in *Spera* [1984]). Unfortunately, however, all laboratory, analytical, and numerical studies of magma withdrawal to date, except for those of *Trial et al.* [1988], are based upon in situ chemical profiles that depend only on the vertical coordinate and ignore lateral variations in magma composition. For sill-like chambers, however, our simulations point out that lateral chemical heterogeneities

can be compositionally significant and long-lived in magma bodies with typical aspect ratios ($1 \leq A \leq 3$). This result points out the potential importance of lateral compositional variations in magma bodies for producing vertically zoned pyroclastic flow deposits. This effect may also be relevant to magma bodies below mid-ocean ridges. If such bodies are characterized by shapes with $A \gg 1$, then one might expect lateral variation in composition to persist for long times. It is possible that the contradicting conclusions of geophysical studies which suggest chambers extend for considerable distances (30 to 150 km) longitudinally beneath ridges [*Macdonald and Fox*, 1988] and geochemical studies which suggest a 10- to 30-km segmentation [*Langmuir et al.*, 1986] can be brought into consistency by considering the convective mixing dynamics in large aspect ratio magma bodies.

Constant influx of hot magma and associated steady heat flux into magma chambers result in shorter mixing times than occur from periodic magma injections and associated pulses of heat, provided the peak heat flux is comparable. The difference, however, does not appear to be great. Sidewall cooling enhances mixing and dictates circulation direction for small Rr. In thermally disconnected magma bodies where cooling occurs out all margins, convective mixing is slow relative to thermally well-connected systems. For equant magma bodies, mixing times are very similar for cases where there is cooling out all margins and where there is cooling out the top. If isolated from heat inputs, magma bodies with large compositional buoyancy ratio and large intensity and scale of segregation can remain heterogeneous for long periods compared with thermally well-connected systems where mixing is more effective. The relative homogeneity of mid-ocean ridge magmas compared with the voluminous and nearly always compositionally zoned epicontinental pyroclastic flow systems may be related to differences in basal thermal boundary conditions.

Exactly how the diffusivities, buoyancy ratio, viscosity ratio, magma body shape, and various thermal boundary conditions will act together to affect the convective mixing process at high $Rq, Rr \gg 1$ is not known. Qualitatively, it appears that the mixing time is approximately proportional to $Rq^{-1}Rr^{2}Le^{1/2}\nu_r^{1/2}$. Caution must be applied in extrapolating from limited simulation studies due to the highly nonlinear character of double-diffusive convection. However, in light of the preponderance of zonation effects in volcanic deposits and plutons, it does appear that the magmatic and the geometric properties of some magmatic systems will act to inhibit magma mixing. AFC modeling studies in which melt is assumed to be homogeneous at all times and at all locations within a body are poor approximations to petrologic reality when $\hat{t}_{mix} > 0.5$. There is no reason to believe, furthermore, that simple (e.g., linearly zoned or multiply layered) patterns of composition will always prevail. Indeed, our results suggest just the opposite; complex patterns of composition through time and space are the rule rather than the exception.

NOTATION

x	horizontal coordinate.
y	vertical coordinate.
u	horizontal velocity.
v	vertical velocity.
q	heat flux.
j	mass flux.
g	acceleration of gravity.
p	pressure.
τ_{ij}	stress tensor.
d	characteristic depth of magma body.
w	characteristic width of magma body.
T	temperature.
C	composition.
α	coefficient of isobaric thermal expansion.
β	coefficient of compositional expansion.
κ	thermal diffusivity.
k	thermal conductivity.
D	chemical diffusivity.
ρ	density.
η_0	dynamic viscosity of mafic melt ($\rho_m \nu_m$).
ν	kinematic viscosity.
B	viscosity coefficient (in eq (16)).
b	viscosity coefficient $b \equiv B\,(C_s - C_m)$.
t	time.
$\dot{V}$	volume rate.
A_c	chamber area.
C_p	heat capacity.
δ	diffusive length scale.
Rq	flux-type Rayleigh number.
Rr	buoyancy ratio.
Le	Lewis number.
ν_r	viscosity ratio.
A	aspect ratio.
Nu	Nusselt number.
σ	standard deviation.
σ^2	variance.
m_3	skewness.
m_4	kurtosis.
L	linear scale of segregation.
V	volume scale of segregation.
L^*	space-correlation linear scale.
$R(r)$	correlation function.
$R^*(r)$	space-correlation function.
I	intensity of segregation.
r	pair separation distance.

Subscripts

b	base.
w	wall.
r	ratio.
m	mafic.
s	silicic.
av	average.
mix	mixing.
0	reference value.

Accented Characters

Circumflex ($\hat{x}$) and overbar ($\bar{x}$) are used to indicate dimensionless variables and spatial average, respectively.

Equivalences

Equivalence symbols used indicate of order ($\sim$), approximately equal to ($\approx$), and equal to ($=$).

Acknowledgments We thank Hossein Moini for help with the preliminary numerical simulations. The staffs of the Minnesota Supercomputer Institute, NASA Ames Research Center, and San Diego Supercomputer Center have been helpful at various times throughout this project. We thank two anonymous reviewers for their comments. This research was supported by NASA (NAGW-1452) and NSF (EAR86-08284) awards to F.J.S. and NASA (NAGW-1008) and NSF (EAR86-08479) awards to D.A.Y. We are grateful to Anne Boyd for her help in preparing this manuscript.

REFERENCES

Bacon, C.R., Eruptive history of Mount Mazama and Crater Lake Caldera, Cascade Range, U.S.A., *J. Volcanol. Geotherm. Res., 18,* 57–115, 1983.

Bacon, C.R., Magmatic inclusions in silicic and intermediate volcanic rocks, *J. Geophys. Res., 91,* 6091–6112, 1986.

Batchelor, G.K., *The Theory of Homogeneous Turbulence,* 242 pp.,Cambridge University Press, New York, 1953.

Bejan, A., and R. Anderson, Natural convection at the interface between a vertical porous layer and an open space, *Trans. ASME, 105,* 124–129, 1983.

Blake, S., Eruptions from zoned magma chambers, *J. Geol. Soc. London, 138,* 281–287, 1981.

Blake, S., and G.N. Ivey, Magma-mixing and the dynamics of withdrawal from stratified reservoirs, J. *Volcanol. Geotherm. Res., 27,* 153–178, 1986*a*.

Blake, S., and G.N. Ivey, Density and viscosity gradients in zoned magma chambers, and their influence on withdrawal dynamics, *J. Volcanol. Geotherm Res., 30,* 201–230, 1986*b*.

Carrigan, C.R., The magmatic Rayleigh number and time dependent convection in cooling lava lakes, *Geophys. Res. Lett., 14(9),* 915–918, 1987.

Clark, S., F.J. Spera, and D.A. Yuen, Steady state double-diffusive convection in magma chambers heated from below, in *Magmatic Processes: Physiochemical Principles* (edited by) B.O. Mysen, Geochemical Society, *Spec. Pub., 1*289–305, 1987.

Crisp, J. A., Rates of magma emplacement and volcanic output, *J. Volcanol. Geotherm. Res., 20,* 177–211, 1984.

Crisp, J.A., and F.J. Spera, Pyroclastic flows and lavas of the Mogan and Fataga formations, Tejeda Volcano, Gran Canaria, Canary Islands: Mineral chemistry, intensive parameters and magma chamber evolution, *Contrib. Mineral. Petrol., 96,* 503–518, 1987.

Danckwerts, P.V., The definition and measurement of some characteristics of mixtures, *Appl. Sci. Res., A3,* 279–296, 1952.

Dowty, E., and C.A. Berkebile, Differentiation and diffusion in laboratory charges of basaltic composition during melting experiments, *Am. Mineral., 67,* 900–906, 1982.

Dungan, M.A., Open system magmatic evolution of the Taos Plateau Volcanic Field, northern New Mexico, II The genesis of cryptic hybrids, *J. Petrol., 28,* 955–977, 1987.

Eichelberger, J.C., Origin of andesite and dacite: Evidence of mixing at Glass Mountain in CA and at other circum-Pacific volcanoes, *Geol. Soc. Am. Bull., 86,* 1381–1391, 1975.

Freundt, A., and S.R. Tait, The entrainment of high-viscosity magma into low-viscosity magma in eruption conduits, *Bull Volcanol., 48,* 325–339, 1986.

Frost, T.P., and G.A. Mahood, Field, chemical, and physical constraints on mafic-felsic magma interaction in the Lamarck Granodiorite, Sierra Nevada, CA, *Geol. Soc. Am. Bull., 99,* 272–291, 1987.

Furman, T., and F.J. Spera, Commingling of acid and basic magma and implications for the origin of I-type xenoliths, I Field and petrochemical relations of an unusual dike complex at Eagle Lake, Sequoia National Park, California, USA, *J. Volcanol. Geotherm. Res., 24,* 151–178, 1985.

Gibson, I.L., and G.P.L. Walker, Some composite rhyolite/basalt lavas and related composite dykes in eastern Iceland, *Proc. Geol. Soc. London, 74,* 301–318, 1963.

Green, N.L., Basalt-basaltic andesite mixing at Mount Baker Volcano, Washington, I Estimation of mixing conditions, *J. Volcanol. Geotherm. Res., 34,* 251–265, 1988.

Grove, T.L., R.J. Kinzler, M.B. Baker, J. Donelly-Nolan, and C.E. Lesher, Assimilation of granitic crust by basaltic magma at Burnt Lava flow, Medicine Lake Volcano, northern California: Decoupling of heat and mass transfer, *Contrib. Mineral. Petrol.,* in press.,1989.

Gurnis, M., and G.F. Davies, Mixing in numerical models of mantle convection incorporating plate kinematics, *J Geophys. Res., 91,* 6375–6395, 1986.

Hansen, U., and D.A. Yuen, Evolutionary structures in double-diffusive convection in magma chambers, *Geophys. Res. Lett., 14* , 1099–1102, 1987.

Hardee, H.C., Incipient magma chamber formation as a result of repetitive intrusions, *Bull Volcanol., 45,* 41–49, 1982.

Hibbard, M.J., The magma mixing origin of mantled feldspars, *Contrib. Mineral. Petrol., 76,* 158–170, 1981.

Hildreth, W., The Bishop Tuff: Evidence for the origin of compositional zonation in silicic magma chambers, *Spec. Pap. Geol. Soc. Am., 180,* 1979.

Hildreth, W., Gradients in silicic magma chambers: Implications for lithospheric magmatism, *J. Geophys. Res., 86,* 10,153–10,193, 1981.

Hildreth, W., The compositionally zoned eruption of 1912 in the Valley of 10^4 Smokes, Katmai National Park, Alaska, *J. Volcanol. Geotherm. Res., 18,* 1–56, 1983.

Hoffman, N.R.A., and D.P. McKenzie, The destruction of geochemical heterogeneities by differential fluid motions during mantle convection, *Geophys. J. R. Astron. Soc., 82,* 163–206, 1985.

Huppert, H.E., and R.S. Sparks, The fluid dynamics of a basaltic magma chamber replenished by influx of hot dense ultra basic magma, *Contrib. Mineral. Petrol., 75,* 279–289, 1980.

Jarvis, G.T., Time-dependent convection in the earth's mantle, *Phys. Earth Planet. Inter., 36,* 305–327, 1984.

Kouchi, A., and I. Sunagawa, Mixing basaltic and dacitic magmas by forced convection, *Nature, 304,* 527–528, 1983.

Langmuir, C.H., J.F. Bender, and R. Batiza, Petrologic and tectonic segmentation of the East Pacific Rise, 5°30'–14°30'N, *Nature, 322,* 422–429, 1986.

Lighthill, M.J., Theoretical considerations on free convection in tubes, *Q. J. Mech. Appl. Math., VI* , 398–439, 1953.

Lowell, R.P., Double-diffusive convection in partially molten silicate systems: Its role during magma production and in magma chambers, *J. Volcanol. Geotherm. Res., 26,* 1–24, 1985.

Macdonald, K.C., and P.J. Fox, The axial summet graben and cross-sectional shape of the East Pacific Rise as indicators of axial magma chambers and recent volcanic eruptions, *Earth Planet. Sci. Lett., 88,* 119–131, 1988.

Marsh, B.D., and M.R. Maxey, On the distribution and separation of crystals in convecting magma, *J. Volcanol. Geotherm. Res., 24,* 95–150, 1985.

Martin, D., and I.C. Campbell, Laboratory modelling of convection in magma chambers: Crystallization against sloping floors, *J. Geophys. Res., 93,* 7974–7988, 1988.

Martin, D., and I.C. Campbell, Laboratory modelling of convection in magma chambers: Crystallization against sloping floors, *J. Geophys. Res., 93,* 7974–7988, 1988.

McBirney, A.R., Mixing and unmixing of magmas, *J. Volcanol. Geotherm. Res., 7,* 357–371, 1980.

McBirney, A.R., B.H. Baker, and R.H. Nilson, Liquid fractionation I, Basic principles and experimental simulations, *J. Volcanol. Geotherm. Res., 24,* 1–24, 1985.

McKenzie, D., Finite deformation during fluid flow, *Geophys. J. R. Astron. Soc., 58,* 689–715, 1979.

Nilson, R.H., A.R. McBirney, and B.H. Baker, Liquid fractionation II, Fluid dynamics and quantitative implications for magmatic systems, *J. Volcanol. Geotherm. Res., 24,* 25–54, 1985.

Nixon, G.T., Petrology of the younger andesites and dacites of Iztaccihuatl Volcano, Mexico, I Disequilibrium phenocryst assemblages as indicators of magma chamber processes, *J. Petrol., 29,* 213–264, 1988*a*.

Nixon, G.T., Petrology of the younger andesites and dacites of Iztaccihuatl Volcano, Mexico, II Chemical stratigraphy, magma mixing and the composition of basaltic magma influx, *J. Petrol., 29,* 265–303, 1988*b*.

Norton, D.L., and J.E. Knight, Transport phenomena in hydrothermal systems: Cooling plutons, *Am. J. Sci., 277,* 937–981, 1977.

O'Brien, H.E., A.J. Irving, and I.S. McCallum, Complex zoning and

resorption of phenocrysts in mixed potassic mafic magmas of the Highwood Mountains, Montana, *Am. Mineral.*, in press, 1989.
Olson, P.M., An experimental approach to thermal convection in a two-layered mantle, *J. Geophys. Res., 89,* 11,293–11,301, 1984.
Olson, P., and D.A. Yuen, and D.S. Balsiger, Convective mixing and the fine structure of mantle heterogeneity, *Phys. Earth Planet. Inter., 36,* 291–304, 1984*a*.
Olson, P., D.A. Yuen, and D. S. Balsiger, Mixing of passive heterogeneities by mantle convection, *J. Geophys. Res., 89,* 425–436, 1984*b*.
Ottino, J.M., and R. Chella, Laminar mixing of polymeric liquids: A brief review and recent theoretical developments, *Polymer Eng. Sci., 23,* 357–379, 1983.
Pallister, J.S., and C.A. Hopson, Samail Ophiolite plutonic suite: Field relations, phase variation, cryptic variation and layering, and a model of a spreading ridge magma chamber, *J. Geophys. Res., 86,* 2593–2644, 1981.
Reagan, M.K., J.B. Gill, E. Malvassi, and M.O. Garcia, Changes in magma composition at Arenal Volcano, Costa Rica, 1968–1985: Real-time monitoring of open-system differentiation, *Bull. Volcanol., 49,* 21–40, 1987.
Richter, F. M., S.F. Daly, and H.- C. Nataf, A parameterized model for the evolution of isotopic heterogeneities in a convecting system, *Earth Planet. Sci. Lett., 60,* 178–194, 1982.
Sewell, G., *Analysis of a Finite Element Method PDE/PROTRAN,* 154 pp., Springer-Verlag, New York, 1985.
Shaw, H.R., Comments on viscosity, crystal settling and convection in granitic systems, *Am. J. Sci., 272,* 120–152, 1965.
Shaw, H.R., Viscosities of magmatic silicate liquids: An empirical method of prediction, *Am. J. Sci., 272,* 870–893, 1972.
Shaw, H.R., Mantle convection and volcanic periodicity in the Pacific: Evidence from Hawaii, *Geol. Soc. Am. Bull., 84,* 1505–1526, 1973.
Shaw, H.R., Diffusion of H_2O in granitic liquids, I, Experimental Data; II, Mass transfer in magma chambers, in *GeochemicalTransport Kinetics,* edited by A.W. Hofmann, B.J. Gilletti, H.S. Yoder, and R.A. Yund, pp. 139–170, Carnegie Institution of Washington, Washington, D.C., 1974.
Smith, R.L., Ash-flow magmatism, *Spec. Pap. Geol. Soc. Am., 180,* 5–28, 1979.
Sparks, R.S.J., and L.A. Marshall, Thermal and mechanical,constraints on mixing between mafic and silicic magmas, *J. Volcanol. Geotherm. Res., 29,* 99–124, 1986.
Spera, F.J., D.A. Yuen, and S.J. Kirshvink, Thermal boundary layer convection in silicic magma chambers: Effects of temperature dependent rheology and implications for thermogravitational chemical fractionation, *J. Geophys. Res., 87,* 8755–8767, 1982.
Spera, F.J., Some numerical experiments on the withdrawal of magma from crustal reservoirs, *J. Geophys. Res., 89,* 8222–8236, 1984.
Spera, F.J., D. A. Yuen, and D.V. Kemp, Mass transfer rates along vertical walls in magma chambers and marginal upwelling, *Nature, 310,* 764–767, 1984.
Spera, F.J., D.A. Yuen, J.C. Greer, and G. Sewell, Dynamics of magma withdrawal from stratified chambers, *Geology, 14,* 723–726, 1986.
Spera, F.J., A. Borgia, J. Strimple, and M. Feigenson, Rheology of melts and magmatic suspensions, I Design, calibration and operation of concentric cylinder viscometer and application to rhyolitic magma, *J. Geophys. Res., 93,* 10,273–10,294, 1988.
Taylor, G.I., Statistical theory of turbulence, *Proc. R. Soc. London, Ser. A, 151,* 421–478, 1935.
Trial, A. F., and F.J. Spera, Natural convection boundary layer flows in isothermal ternary systems: Role of diffusive coupling, *Int. J. Heat Mass Transfer, 31,* 941–955, 1988.
Trial, A.F., F.J. Spera, and D.A. Yuen, Effect of non-Newtonian rheology on the withdrawal of magma from a stratified chamber, *Eos Trans. AGU, 69,* 525, 1988.
Turner, J.S., A fluid dynamical model of differentiation and layering in magma chambers, *Nature, 285,* 213–215, 1980.
Turner, J.S., Multicomponent convection, *Annu. Rev. Fluid Mech., 17,* 11–44, 1985.
Turner, J.S., and I.H. Campbell, Convection and mixing in magma chambers, *Earth Sci. Rev., 23,* 255–352, 1986.
Urbain, G., Y. Bottinga, and P. Richet, Viscosity of liquid silica, silicates and alumino-silicates, *Geochim. Cosmochim. Acta, 46,* 1061–1072, 1982.
Vernon, R.H., Restite, xenoliths and microgranitoid enclaves in granites, *R. Soc. New S. Wales J. Proc., 116,* 77–103, 1983.
Walker, G.P.L., and R.R. Skelhorn, Some associations of acid and basic igneous rocks, *Earth Sci. Rev., 2,* 93–109, 1966.
Weinstein, S.A., D.A. Yuen, and P.L. Olson, Evolution of crystal settling in magma-chamber convection, *Earth Planet. Sci. Lett., 87,* 237–248, 1987.
Wiebe, R.A., Plagioclase stratigraphy: A record of magmatic conditions and events in granitic stock, *Am. J. Sci., 266,* 690–703, 1968.
Wiebe, R.A., Relations between coexisting basaltic and granitic magmas in a composite dike, *Am J. Sci., 273,* 130–151, 1973.
Wiebe, R.A., Coexisting intermediate and basic magmas, Ingonish, Cape Breton Island, *J. Geol., 82,* 74–87, 1974.
Wiebe, R.A., Commingling of contrasted magmas in the plutonic environment: Examples from the Nain anorthostic complex, *J. Geol., 88,* 197–209, 1980.
Wiebe, R.A., Structural and magmatic evolution of a magma chamber: The Newark Island Layered Intrusion, Nain, Labrador, *J. Petrol., 29,* 383–411, 1988.
Wilcox, R.E., Petrology of Paricutin Volcano, Mexico, *US Geol. Surv. Bull., 965-C,* 1954.
Wright, T.L., Magma mixing as illustrated by the 1959 eruption, Kilauea Volcano, Hawaii, *Geol. Soc. Am. Bull., 84,* 849–858, 1973.

C.M. Oldenburg and F.J. Spera, Department of Geological Sciences, Universtiy of California, Santa Barbara, CA 93106.
G. Sewell, Department of Mathematical Sciences, University of Texas, El Paso, TX 79968.
D.A. Yuen, Minnesota Supercomputer Institute and Department of Geology, Universtiy of Minnesota, Minneapolis, MN 55455.

(Received April 7, 1988;
revised July 13, 1988;
accepted October 31, 1988.)